

Bosonization approach to charge and spin dynamics of 1D fermions with band-curvature

Sofian Teber

The Abdus Salam ICTP, Strada Costiera 11, 34014, Trieste, Italy

(Dated: May 25, 2019)

We consider one-dimensional (1D) spin-1/2 fermions in a clean quantum wire, with forward scattering interactions and a non-linear single-particle spectrum, $\xi_k = v|k| + k^2/2m$ where v is the Fermi velocity and $1/m$ is the band-curvature. We calculate the dynamical structure factor (DSF) of the model at small wave-vector q with the help of the bosonization technique. Being perturbative in band-curvature with singular perturbations, bosonization cannot emulate the 2-parametric excitation spectrums starting from the single-parametric ones: $\omega = u_{\rho,\sigma}|q|$ where $u_\rho \geq u_\sigma$ are the charge and spin velocities, respectively. On the other hand, away from the excitation-cones, *i.e.* $\omega \gg u_{\rho,\sigma}|q|$, bosonization yields the 2-pair excitation continuum of the DSF. For $u_\rho > u_\sigma$, spin-charge coupling (SCC) due to band-curvature affect charge and spin DSF in an asymmetric way. For the charge DSF, SCC manifests as a two-peak structure: a charge peak at $\omega = u_\rho|q|$ but also a spin peak at $\omega = u_\sigma|q|$, as charge fluctuations may decay via chargeless spin-singlet excitations. For the magnetic DSF, SCC manifests as a continuous transfer of magnetic spectral weight to frequencies $\omega > u_\sigma|q|$, as spin fluctuations decay via pairs of chargeless spin and spinless charge-neutral excitations.

I. INTRODUCTION

Correlation functions of one-dimensional (1D) fermions in quantum wires are conveniently calculated within the *Tomonaga-Luttinger* (TL) *model* and with the help of the bosonization technique. The TL model assumes the linearity of the single-particle spectrum with respect to momentum:

$$\xi_k = v(|k| - k_F) \quad (\text{Tomonaga - Luttinger}), \quad (1)$$

where v is the Fermi velocity and k_F the Fermi momentum, and interactions of the forward scattering type, so-called g_2 and g_4 processes in g -ology. The forward scattering nature of the interactions implies that the system has no spectral gap whereas the linearity of the spectrum yields Lorentz invariance. These assumptions make the model exactly soluble by mapping the interacting fermions onto free bosonic excitations or plasmons [1,2,3,4]. As a consequence, *e.g.* transport, properties of TL liquids are easily accessed with the help of bosonization, see the recent monographs [5,6].

Even though the TL model allows a standard description of fermions in quantum wires, as Landau theory of Fermi liquids allows a standard description of 3D systems, *cf.* the monograph [7], both assumptions of relativistic single-particle spectrum and forward scattering interactions often constitute an over simplified description of 1D fermionic systems. As a matter of fact, fermions hopping with an amplitude t on a 1D lattice of parameter a have a single-particle spectrum given by:

$$\xi_k = -2t \cos(ka) \quad (\text{Hubbard}). \quad (2)$$

Adding interactions between such fermions leads to the *1D Hubbard model*, see the monograph [8], one of the most fundamental model of solid-state physics. In the absence of disorder and away from 1/2-filling we may

assume that the system has no spectral gap, *e.g.* is not in a Mott insulating phase. One may then focus on the low-energy properties of this model by expanding Eq. (2) around the Fermi points $\pm k_F$ where the + sign refers to right-movers and the - sign to left-movers. In the lowest order, this yields the TL model, Eq. (1), with $v = 2ta \sin(k_F a)$. Because of the exact solubility of the TL model the low-energy properties of the Hubbard model are thus known exactly. On the other hand, except for the case of free fermions which is again exactly soluble, less is known about the high-energy properties of the Hubbard model. Considerable work has been devoted to exact studies related to the nature of its ground-state and its low-energy excitations. This has been done with the help of the *Bethe Ansatz*, *cf.* [8,9] for reviews, which allows a fully non-perturbative handling of the non-linear spectrum, Eq. (2), and interaction effects. This technique is however extremely difficult to generalize to the calculation of correlation functions. Formidable efforts are made to achieve this task but they are limited at present to the 1/2-filled case [10] and to the XXZ Heisenberg spin-chain, see [11] for a review (the XXZ spin-chain is equivalent to spinless fermions, *cf.* Ref. [12] for a review on spin-chains and the Hubbard model).

In this contribution we focus on a different approach to the high-energy properties of strongly correlated 1D fermions. This amounts to start from the TL model, assume forward scattering interactions and introduce band-curvature corrections to the linear single-particle spectrum:

$$\xi_k = v(|k| - k_F) + (|k| - k_F)^2/2m, \quad (3)$$

where $m = k_F/v$ is the band-mass or, equivalently, $1/m$ is the band-curvature. For Galilean invariant systems, there are no higher order corrections in band-curvature. On the other hand, for lattice fermions, Eq. (3) only retains the most relevant, *i.e.* first-order,

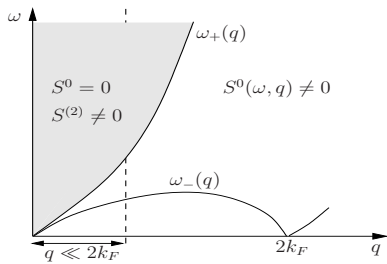


FIG. 1: Schematic view on the spectrum of excitations of 1D spinless fermions. The free-fermion, or single-pair excitation continuum S^0 , lies between the ω_- and ω_+ branches. In the presence of forward scattering interactions a multi-pair excitation continuum ($S^{(2)}$ at the 2-pair level) spreads above the ω_+ branch.

band-curvature correction to the single-particle spectrum in the expansion around the Fermi points: $\pm k_F$, see Eq. (2). This means that, with respect to the Hubbard model, the model defined by Eq. (3) is essentially perturbative in band-curvature even if we solve it exactly. Despite this limitation such a model allows to extract information about dynamical correlation functions of 1D fermions with band-curvature and interactions. This is a basic step *beyond* the TL model and *towards* the Hubbard model. Up to now it has been mainly considered for the case of spinless fermions, see Refs. [4,14,15,16,17,18,19,20,21] or for the equivalent XXZ Heisenberg spin-chain, see Refs. [19,20].

The main results of these work show that, on a perturbative level, the band-curvature corrections of Eq. (3) mainly affect the high-energy, *e.g.* high-frequency, properties of the system preserving its Luttinger-like features at low-energies, see [15,18,19,20,21]. On the other hand, on a non-perturbative level, the band-curvature corrections of Eq. (3) cure the system from strong divergences present within the TL approximation, *e.g.* thereby realistically yielding a finite life-time for the elementary excitations of the liquid, see [14,15,18,19,20]. The latter may be seen for the case of free-fermions by considering the density-density correlation function or polarization operator:

$$\Pi(x, \tau) = \langle \rho(x, \tau) \rho(0, 0) \rangle,$$

where ρ is the fermion density measured relative to a neutralizing jellium. For free-fermions this correlation function is known exactly with band-curvature and, in Fourier space, reads:

$$\Pi^0(i\omega, q) = \frac{m}{2\pi q} \ln \left[\frac{(i\omega)^2 - (\omega_-)^2}{(i\omega)^2 - (\omega_+)^2} \right], \quad (4)$$

where the upper index refers to free-fermions and the 2-parametric family appears:

$$\omega_{\pm}(q) = vq \pm \frac{q^2}{2m}. \quad (5)$$

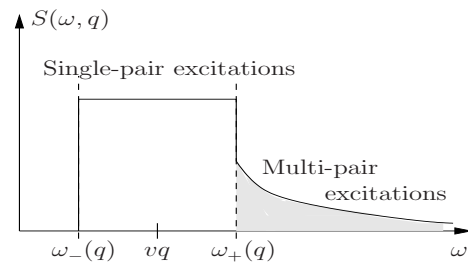


FIG. 2: Schematic view on the dynamical structure factor of spinless fermions as a function of frequency ω for a given momentum q , *e.g.* the cut at $q \ll 2k_F$ of Fig. 1. The free-fermion or single-pair excitation continuum lies between the ω_- and ω_+ branches. The 2- and higher-pair excitation continuum due to interactions lie beyond the ω_+ branch.

In the excitation spectrum of the system this family bounds the region of decay of the coherent bosonic excitation, the plasmon which corresponds to a coherent particle-hole pair, into the incoherent continuum of single particle-hole pairs, see Fig. 1. This is best revealed by looking at the dynamic structure factor (DSF) of the fermions which corresponds to the dissipative part of the retarded polarization operator:

$$S(\omega, q) = -\Im \Pi^R(\omega, q). \quad (6)$$

For free fermions, Eqs. (4) and (6) yield:

$$S^0(\omega, q) = \frac{m}{2|q|} \left[\theta\left[\frac{mv}{q}(\omega - \omega_-)\right] - \theta\left[\frac{mv}{q}(\omega - \omega_+)\right] \right] - \{\omega \rightarrow -\omega\}, \quad (7)$$

which, for a fixed momentum q , is non-zero and independent on frequency in the range: $\omega_- < \omega < \omega_+$, see Fig. 2. In particular, at the plasmon frequency Eq. (7) yields a finite result:

$$S^0(\omega = vq, q) = m/2|q|. \quad (8)$$

Moreover, the spectral width of the DSF yields the inverse life-time of the bosonic excitations:

$$\delta\omega = |\omega_+ - \omega_-| = \frac{q^2}{m}. \quad (9)$$

On the other hand, expanding Eq. (4) in $1/m$ yields:

$$\begin{aligned} \Pi^0(i\omega, q) & \\ &= \frac{1}{\pi v} \sum_{n=0}^{\infty} \frac{1}{2n+1} \left(\frac{q^2}{m}\right)^{2n} \frac{(vq)^{2n+2}}{[(i\omega)^2 - (vq)^2]^{2n+1}}, \end{aligned} \quad (10)$$

which reveals a basic difference with respect to the exact result of Eq. (4): order by order the dissipative part is singular at the plasmon frequency: $\omega = v|q|$, with δ -function singularities. In particular, within the TL approximation ($m \rightarrow \infty$):

$$S_{TL}^0(\omega, q) = \frac{|q|}{2} \delta[\omega - v|q|], \quad (11)$$

which implies that plasmons have an infinite life-time, *i.e.* are free. The divergency of the DSF, in the limit $m \rightarrow \infty$, agrees with Eq. (8) but the nature of the divergency is different according to the order with which the limits $m \rightarrow \infty$ and $\omega \rightarrow vq$ are taken. The fact that these limits do not commute and the strong divergences which affect the TL liquid witness the difficulty to emulate the 2-parametric family of Eq. (5) starting from the single-parametric one: $\omega = v|q|$. Band-curvature indeed cures the δ -function singularities, *cf.* Eq. (8), and provides the finite life-time of the elementary excitations, *cf.* Eq. (9), but only after summing over an infinite number of singular terms.

Our goal is to calculate the DSF (at small q , *i.e.* the $2k_F$ -part is not considered) with band-curvature with the help of the bosonization technique. The latter allows to take forward scattering interactions among the fermions to all orders. Bosonization, as a standard low-energy Lorentz invariant field theory technique, is based on the assumption of a linear single-particle spectrum. Starting with spinless fermions we will extend it to the case where band-curvature is present. This will make the bosonization non-linear a signature that the low-energy bosonic excitations interact. Our first task will then be to determine whether or not this (non-linear) bosonization is able to cure itself from its divergences with the help of the curvature corrections of Eq. (3). We will also evaluate the effect of interactions on the DSF with band-curvature, *cf.* the high frequency multi-pair excitation continuum displayed on Figs. 1 and 2. This complements existing works in the literature on the subject [4,14,15,18,19,20,21] in particular those using bosonization [4,14,20]. Next, by considering spinful fermions (with spin-1/2) we will explore some features related to the violation of the spin-charge separation due to band-curvature. Within bosonization, this was first considered in Ref. [13] that we shall follow (correlation functions were not the main issue of Ref. [13]). We understand this violation as follows. As known from the Bethe Ansatz solution to the Hubbard model, *cf.* Refs. [8,9] for reviews, in the presence of band-curvature spin-charge decoupling is still valid at the level of the elementary excitations: they consist of the chargeless spin-1/2 spinon and the spinless charged holon and anti-holon²². This is also valid for the physical excitations²³ composed of the elementary ones (particle-hole pairs, spin-singlet and triplet) and living in either sector. However, because of band-curvature they interact with each-other as well as, below half-filling, with the background charge living in the wire²⁴. As a consequence, spin and charge Hilbert spaces are no more separated at high energies and the excitations acquire a finite life-time. We will explore the effect of this coupling on the charge and spin density correlation functions of the model which, to our knowledge, has not been done elsewhere.

The paper is structured as follows. In Sec. II we introduce the model of bosonized spinless fermions with band curvature, calculate the corresponding DSF at small q

and discuss the efficiency of the non-linear bosonization technique. In Sec. III we add an additional internal, spin-1/2, degree of freedom to the fermions. We calculate the charge and magnetic DSF, both at small q , and discuss the violation of the spin-charge separation due to band curvature for both functions. In Sec. IV we summarize our results and conclude. Finally some details of the calculations are reported in the Appendices at the end of the paper.

II. SPINLESS FERMIONS

A. Model

In this Section, we consider spinless fermions and give some details of the standard bosonization procedure. Starting with free fermions their Hamiltonian reads:

$$H = \sum_k \xi_k : c_k^\dagger c_k :,$$

where c and c^\dagger are the annihilation and creation operators for the fermions and $::$ refers to normal ordering. The bosonization procedure is implemented by first focusing on the low-energy sector near the Fermi points $\pm k_F$:

$$c(x) \sim \psi_+(x)e^{ik_F x} + \psi_-(x)e^{-ik_F x},$$

where ψ_\pm are slow chiral fields. The free fermion Hamiltonian becomes:

$$H = iv \int dx \left[: \psi_+^\dagger \partial_x \psi_+ : - : \psi_-^\dagger \partial_x \psi_- : \right] - \frac{1}{2m} \int dx \left[: \psi_+^\dagger \partial_{xx} \psi_+ : + : \psi_-^\dagger \partial_{xx} \psi_- : \right]. \quad (12)$$

The first term corresponds to the Dirac part related to the linear spectrum. The second term corresponds to the curvature correction. One may then go to the bosonic representation with the help of the following identity:

$$\psi_\pm(x) = \frac{1}{\sqrt{2\pi}} : \exp \left[\pm i\sqrt{4\pi} \varphi_\pm(x) \right] :, \quad (13)$$

relating the chiral fermionic fields, ψ_\pm , to the chiral bosonic fields, φ_\pm . The later may be expressed as a function of the total phase field φ and the momentum Π_φ as follows:

$$\varphi_\pm = \frac{1}{2} \left(\varphi \mp \int_{-\infty}^x dx' \Pi_\varphi(x') \right). \quad (14)$$

The normal-ordering of vertex operators is conveniently taken into account with the help of a point-splitting technique, see details in Appendix A. This yields the following operator-product expansions ($\eta = \pm$):

$$\begin{aligned} \psi_\eta^\dagger(x)\psi_\eta(x) &= -\frac{1}{\sqrt{\pi}} \partial_x \varphi_\eta(x), \\ \psi_\eta^\dagger(x)\partial_x \psi_\eta(x) &= -i \operatorname{sgn}(\eta) : (\partial_x \varphi_\eta(x))^2 :, \\ \psi_\eta^\dagger(x)\partial_{xx} \psi_\eta(x) &= \frac{4\sqrt{\pi}}{3} : (\partial_x \varphi_\eta(x))^3 :, \end{aligned} \quad (15)$$

where the terms which vanish upon integration over space or by symmetry considerations have been neglected. The last line in Eq. (15) displays the non-linearity of the bosonization arising from band-curvature. The fermionic Hamiltonian then takes over the following form:

$$H = v \int dx [(\partial_x \varphi_+)^2 + (\partial_x \varphi_-)^2] - \frac{2\sqrt{\pi}}{3m} \int dx [(\partial_x \varphi_+)^3 + (\partial_x \varphi_-)^3], \quad (16)$$

with the densities:

$$\rho_+(x) = -\frac{1}{\sqrt{\pi}} \partial_x \varphi_+(x), \quad \rho_-(x) = -\frac{1}{\sqrt{\pi}} \partial_x \varphi_-(x).$$

The fact that the curvature part is cubic in densities is related to the energy of the Fermi sea for a quadratic spectrum in 1D. Moreover, such cubic terms lead to a violation of the particle-hole symmetry, $\varphi_{\pm} \rightarrow -\varphi_{\pm}$, again a consequence of the non-linearity of the spectrum away from half-filling. Finally, notice that the curvature term in Eq. (16) agrees with the one found in the literature [4,14,20], see Appendix B for conventions on notations.

In terms of the total phase and momentum this yields:

$$H = \frac{v}{2} \int dx [\Pi_{\varphi}^2 + (\partial_x \varphi)^2] - \frac{\sqrt{\pi}}{6m} \int dx \partial_x \varphi [3\Pi_{\varphi}^2 + (\partial_x \varphi)^2]. \quad (17)$$

According to phenomenological bosonization the added terms, $(\partial_x \varphi)^3$ and $\partial_x \varphi \Pi_{\varphi}^2$, are the lowest-order particle-hole symmetry violating terms compatible with both the $U(1)$ invariance of the Hamiltonian, *i.e.* $\varphi \rightarrow \varphi + \alpha$ where α generates the translations, and the space-time symmetries of the problem: φ is an odd function of x and an even function of t :

$$\rho = -\frac{1}{\sqrt{\pi}} \partial_x \varphi, \quad j = \frac{1}{\sqrt{\pi}} \partial_t \varphi, \quad (18)$$

where ρ is the total density (the smooth part of the density close to $q = 0$; the $2k_F$ part has been neglected), j the total current of the fermions and $\Pi_{\varphi} \sim \partial_t \varphi$, see Eq. (21) below. Notice also, from Eq. (18), that the original (spinless) fermions correspond to kinks in φ .

To include forward scattering interactions we follow the usual prescription of rescaling the fields:

$$\Pi_{\varphi} \rightarrow \sqrt{\gamma_{\rho}} \Pi_{\varphi}, \quad \varphi \rightarrow \frac{1}{\sqrt{\gamma_{\rho}}} \varphi, \quad v \rightarrow u_{\rho},$$

in the Tomonaga-Luttinger part of the Hamiltonian, where:

$$\gamma_{\rho} = \sqrt{\frac{1 + g_{4,c}/2 - g_{2,c}/2}{1 + g_{4,c}/2 + g_{2,c}/2}},$$

$$u_{\rho} = v \sqrt{(1 + g_{4,c}/2)^2 - (g_{2,c}/2)^2},$$

and $g_{i,c} \equiv g_{i,c}/\pi v$ is the dimensionless coupling constant in the charge sector. In the following we take: $g_{2,c} = g_{4,c} = g_c$ which yields:

$$\gamma_{\rho} = \frac{1}{\sqrt{1 + g_c}}, \quad u_{\rho} = v \sqrt{1 + g_c}. \quad (19)$$

The interactions affect the free fermion Hamiltonian density as:

$$\mathcal{H} = \frac{u_{\rho}}{2} \left[\gamma_{\rho} \Pi_{\varphi}^2 + \frac{1}{\gamma_{\rho}} (\partial_x \varphi)^2 \right] - \frac{\sqrt{\pi}}{6m} \partial_x \varphi [3\Pi_{\varphi}^2 + (\partial_x \varphi)^2]. \quad (20)$$

To proceed further, we find it more convenient to go to the Lagrangian representation, $\Pi_{\varphi} \rightarrow \partial_x \theta$, which yields the following Euclidean action:

$$S_E = \int d\tau dx \left[\frac{u_{\rho} \gamma_{\rho}}{2} \left[1 - \frac{6}{m' u_{\rho} \gamma_{\rho}} \partial_x \varphi \right] (\partial_x \theta)^2 - i \partial_x \theta \partial_{\tau} \varphi + \frac{u_{\rho}}{2\gamma_{\rho}} (\partial_x \varphi)^2 - \frac{1}{m'} (\partial_x \varphi)^3 \right],$$

where $m' = 6m/\sqrt{\pi}$ and $\tau = it$ is the imaginary time. Integrating over the dual phase field θ yields:

$$\mathcal{L}_E[\varphi] = \frac{1}{2\gamma_{\rho} u_{\rho}} \frac{1}{1 - \frac{6}{m' u_{\rho} \gamma_{\rho}} \partial_x \varphi} (\partial_{\tau} \varphi)^2 + \frac{u_{\rho}}{2\gamma_{\rho}} (\partial_x \varphi)^2 - \frac{1}{m'} (\partial_x \varphi)^3.$$

The non-trivial denominator comes from the conjugated momentum which reads:

$$\Pi_{\varphi} = \frac{\partial_t \varphi}{u_{\rho} \gamma_{\rho} \left(1 - \frac{6}{m' u_{\rho} \gamma_{\rho}} \partial_x \varphi \right)}. \quad (21)$$

Expanding the previous expression in the lowest meaningful order in $1/m$ yields:

$$\mathcal{L}_E[\varphi] = \frac{1}{2v} [(\partial_{\tau} \varphi)^2 + u_{\rho}^2 (\partial_x \varphi)^2] + \frac{1}{m' v^2} \partial_x \varphi [3 (\partial_{\tau} \varphi)^2 - v^2 (\partial_x \varphi)^2], \quad (22)$$

where we have used the fact that: $\gamma_{\rho} u_{\rho} = v$, independent of interactions.

As an alternative to Eq. (22), we may work with the complete action:

$$\mathcal{L}_E[\varphi, \theta] = \frac{u_{\rho} \gamma_{\rho}}{2} (\partial_x \theta)^2 + \frac{u_{\rho}}{2\gamma_{\rho}} (\partial_x \varphi)^2 - i \partial_x \theta \partial_{\tau} \varphi - \frac{3}{m'} \partial_x \varphi (\partial_x \theta)^2 - \frac{1}{m'} (\partial_x \varphi)^3, \quad (23)$$

which does not require any expansion in $1/m$.

With the help of Eq. (22) or Eq. (23) we wish to determine the effect of the irrelevant terms appearing due to curvature on the correlation functions of the model. In particular the long-distance part (close to $q = 0$;

the $2k_F$ -part is neglected) of the polarization operator reads:

$$\Pi(x, \tau) = \langle \rho(x, \tau) \rho(0, 0) \rangle = \frac{1}{\pi} \langle \partial_x \varphi(x, \tau) \partial_x \varphi(0, 0) \rangle.$$

From its expression in Fourier space all we need to compute is the phase correlator \mathcal{D} :

$$\Pi(i\omega, q) = -\frac{q^2}{\pi} \mathcal{D}(i\omega, q), \quad \mathcal{D}(i\omega, q) = \langle |\varphi(i\omega, q)|^2 \rangle.$$

Curvature terms make the actions non-Gaussian a signature of the fact that they induce interactions between the bosonic excitations. We will treat them in perturbation theory in $1/m$. Notice that for Eq. (22) curvature generates an infinite number of irrelevant terms and we have taken into account only the lowest order terms. This means that our treatment of curvature is essentially perturbative (even if we manage to re-sum all terms generated by Eq. (22)). At second-order, both models of Eq. (22) and Eq. (23) are equivalent as will be shown in more details below.

B. Dynamical structure factor

We now compute $\mathcal{D}(i\omega, q)$ via bosonization, *i.e.* in perturbation theory in $1/m$. From Eq. (22) the zeroth order reads:

$$\mathcal{D}^{(0)}(i\omega, q) = -\frac{u_\rho \gamma_\rho}{(i\omega)^2 - (u_\rho q)^2}, \quad (24)$$

from which:

$$\Pi^{(0)}(i\omega, q) = \frac{\gamma_\rho}{\pi u_\rho} \frac{(u_\rho q)^2}{(i\omega)^2 - (u_\rho q)^2}, \quad (25)$$

which agrees with the zero order term of Eq. (10) in the free-fermion limit: $\gamma_\rho = 1$ and $u_\rho = v$.

In the Euclidean action the cubic perturbation reads:

$$S_E = \frac{i}{m' v^2} \frac{1}{\beta^3} \sum_{\omega_1, \omega_2, \omega_3} \int \frac{dq_1 dq_2 dq_3}{(2\pi)^3} \delta[1 + 2 + 3] \\ [3 q_1 \omega_2 \omega_3 - v^2 q_1 q_2 q_3] \varphi_{\omega_1}(q_1) \varphi_{\omega_2}(q_2) \varphi_{\omega_3}(q_3).$$

The second-order correction reads:

$$\mathcal{D}^{(2)}(i\omega, q) = \mathcal{D}^{(0)}(i\omega, q) \Sigma(i\omega, q) \mathcal{D}^{(0)}(i\omega, q),$$

where $\Sigma(i\omega, q)$ is the self-energy part. From the expression of the free bosonic Green function, Eq. (24), this yields:

$$\Pi^{(2)}(i\omega, q) = -\frac{\gamma_\rho^2}{\pi} \frac{(u_\rho q)^2}{[(i\omega)^2 - (u_\rho q)^2]^2} \Sigma(i\omega, q).$$

For the φ -Lagrangian the diagrammatic theory assigns a solid line for the bare propagator of Eq. (24) and the second-order self-energy part is displayed on Fig. 3. To

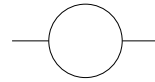


FIG. 3: Second order diagram of the bosonic field theory for the φ -Lagrangian of Eq. (22) for spinless fermions.

compute this self-energy part one has to be careful in Wick ordering the 8-point correlation functions generated by the cubic action at second order. This care is due to the fact that, in the φ -representation, the vertices carry products of frequency and momenta in a non-symmetric way which complicates the calculation of the combinatorial factor (calculations are detailed in Appendix C 1). The latter is crucial as we will see in the following.

As an alternative to the φ -representation we may work in the φ, θ -representation. As we have noticed in Sec. II A the φ -Lagrangian of Eq. (22) is derived by neglecting an infinite number of irrelevant perturbations. On the other hand no such truncation appears in the φ, θ -Lagrangian of Eq. (23). At the second order of the perturbation theory in curvature both approaches should yield the same results while at higher orders the φ, θ -Lagrangian has to be used. Moreover, in the φ, θ -representation the vertices carry products of momentum in a symmetric way which simplifies the Wick ordering at the expense of having more diagrams to evaluate. The latter can be seen from the Fourier transform of Eq. (23) which yields the following perturbations:

$$S_E = -\frac{i}{m'} \frac{1}{\beta^3} \sum_{\omega_1, \omega_2, \omega_3} \int \frac{dq_1 dq_2 dq_3}{(2\pi)^3} \delta[1 + 2 + 3] \\ q_1 q_2 q_3 [3 \varphi_{\omega_1}(q_1) \theta_{\omega_2}(q_2) \theta_{\omega_3}(q_3) + \varphi_{\omega_1}(q_1) \varphi_{\omega_2}(q_2) \varphi_{\omega_3}(q_3)].$$

The quadratic part of Eq. (23) yields the zero-order correlators:

$$\mathcal{D}_{\varphi\varphi}^{(0)}(i\omega, q) = \langle |\varphi(i\omega, q)|^2 \rangle = -\frac{u_\rho \gamma_\rho}{(i\omega)^2 - (u_\rho q)^2}, \\ \mathcal{D}_{\theta\theta}^{(0)}(i\omega, q) = \langle |\theta(i\omega, q)|^2 \rangle = -\frac{u_\rho}{\gamma_\rho} \frac{1}{(i\omega)^2 - (u_\rho q)^2}, \\ \mathcal{D}_{\varphi\theta}^{(0)}(i\omega, q) = \langle \varphi(i\omega, q) \theta(-i\omega, -q) \rangle = \frac{-i\omega}{q[(i\omega)^2 - (u_\rho q)^2]}, \\ \mathcal{D}_{\theta\varphi}^{(0)}(i\omega, q) = \mathcal{D}_{\varphi\theta}^{(0)}(i\omega, q). \quad (26)$$

Notice that while the charge phase φ is related to particle-hole pairings, $\mathcal{D}_{\varphi\varphi}^{(0)} \sim \Pi^{(0)}$, its dual, θ , is a "superconducting" phase and $\mathcal{D}_{\theta\theta}^{(0)}$ is related to particle-particle pairings. The fact that φ and θ appear on equal footing in Eq. (22) is related to the absence of long-range order (either of the charge-density wave type or the superconducting one) in 1D.

The diagrammatic theory then assigns a solid line for the φ -field and a double line for the θ -field, see Fig. 4. Expanding the perturbation up to second order and Wick ordering the 8-point correlation functions yields seven different types of diagrams represented on

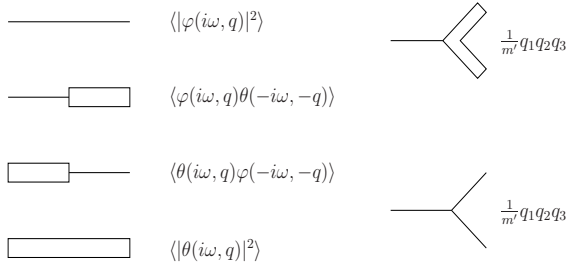


FIG. 4: The quantum field theory associated with the φ, θ -Lagrangian of Eq. (23) for spinless fermions.

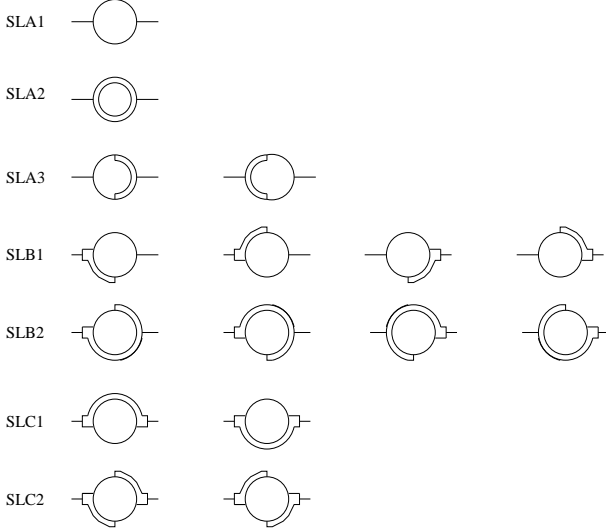


FIG. 5: Second order diagrams of the bosonic field theory for the φ, θ -Lagrangian of Eq. (23) for spinless fermions. SL stands for: Spin Less. The sets of diagrams SLA, SLB and SLC are analyzed in Appendix C 2.

Fig. 5. They are classified according to the number of θ -wings attached to the self-energy parts, see Appendix C 2 for the details. These diagrams, Fig. 5, yield exactly the same self-energy contribution as the one of the φ -representation, Fig. 3.

The final result for the small q self-energy reads (at $T = 0$ for simplicity):

$$\Im \Sigma_{\rho}^R(\omega, q) = \quad (27)$$

$$\frac{\gamma_{\rho}^2 \pi}{96 u_{\rho}} \left[1 + \frac{3}{\gamma_{\rho}^2} \right]^2 \left(\frac{q^2}{m} \right)^2 u_{\rho} q [\delta[\omega - u_{\rho} q] - \delta[\omega + u_{\rho} q]]$$

$$+ \frac{\gamma_{\rho}^2 \pi}{64 u_{\rho}} \left[1 - \frac{1}{\gamma_{\rho}^2} \right] \left(\frac{q}{m u_{\rho}} \right)^2 [\omega^2 - (u_{\rho} q)^2] \mathcal{F}_{\rho}(\omega, q),$$

where we have restored $m' = 6m/\sqrt{\pi}$ and defined the kinematic factor:

$$\mathcal{F}_{\rho}(\omega, q) = \theta[\omega - u_{\rho} q] - \theta[-\omega - u_{\rho} q]. \quad (28)$$

The self-energy reveals the two interesting cases of free-fermions and interacting fermions, respectively.

In the case of free fermions: $u_{\rho} = v$ and $\gamma_{\rho} = 1$, the self-energy has a single contribution on the "plasmon-cone": $\omega = v|q|$. We may recast it in the Matsubara form for clarity:

$$\Sigma_{\rho}(i\omega, q) = -\frac{1}{3v} \left(\frac{q^2}{m} \right)^2 \frac{(vq)^2}{(i\omega)^2 - (vq)^2},$$

from which the corresponding correction to the polarization operator reads:

$$\Pi^{(2)}(i\omega, q) = \frac{1}{3\pi v} \left(\frac{q^2}{m} \right)^2 \frac{(vq)^4}{[(i\omega)^2 - (vq)^2]^3}.$$

This perfectly agrees with the second-order correction known from the free-fermion result of the Introduction, Eq. (10).

In the case of interacting fermions, Eq. (27) shows that this contribution gets renormalized by interactions and that an additional contribution appears at high frequencies. On the plasmon-cone, $\omega = v|q|$, the self-energy may be again conveniently re-casted in the Matsubara form from which the corresponding correction to the polarization operator reads:

$$\Pi^{(2)}(i\omega, q) = \frac{1}{3\pi u_{\rho}} \left(\frac{q^2}{m_0^*} \right)^2 \frac{(u_{\rho} q)^4}{[(i\omega)^2 - (u_{\rho} q)^2]^3}. \quad (29)$$

Again, this has the same functional form as the free-fermion result up to a re-normalization of the charge velocity and the band-mass by interactions:

$$m_0^* = \frac{4m}{\gamma_{\rho}^2 [1 + 3/\gamma_{\rho}^2]} = m \frac{1 + g_c}{1 + 3g_c/4},$$

where Eq. (19) has been used. Away from the plasmon-cone, $\omega \gg v|q|$, Eq. (27) yields the small wave-vector, high-frequency part of the dynamic structure factor:

$$S_{\rho}^{(2)}(\omega, q) = \frac{1}{64 u_{\rho}} \left(\frac{q^2}{m_1^*} \right)^2 \frac{1}{\omega^2 - (u_{\rho} q)^2} \mathcal{F}_{\rho}(\omega, q). \quad (30)$$

In Eq. (30) the re-normalization of the band-mass by interactions differs from the on-cone part:

$$m_1^* = \frac{m}{\gamma_{\rho}^2 [1 - 1/\gamma_{\rho}^2]} = m \frac{1 + g_c}{g_c},$$

where Eq. (19) has been used. This tail describes the decay of a plasmon into two plasmon excitations as can be seen from the vertices of Fig. 4. In fermionic language the plasmon corresponds to a coherent particle-hole pair. As a consequence the tail is termed the two-pair excitation continuum, see Figs. 1 and 2. Notice that the kinematic factor appearing in Eq. (30), see also Eq. (28), is due to the fact that, in 1D, low-energy particle-hole pairs cannot exist for arbitrarily small momentum.

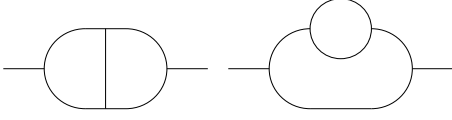


FIG. 6: Fourth order diagrams of the bosonic field theory for the φ -Lagrangian of spinless fermions.

C. Efficiency and limitations of the bosonization technique

As we now discuss, the previous results show that the bosonization technique works well at high-frequencies, *i.e.* $\omega \gg u_\rho|q|$, even though it is limited, because of its non-linearity, to a perturbative evaluation of band-curvature effects. On the other hand it fails at low frequencies, *i.e.* close to the plasmon mode which is on the cone $\omega = u_\rho|q|$, where band-curvature perturbations are singular at all orders and a re-summation of such singular perturbations is non-trivial.

The high-frequency regime manifests only in the presence of curvature *and* interactions. Indeed, in the absence of curvature the bosonic excitations are free and there is no dissipation even though the underlying fermions strongly interact. On the other hand, in the absence of interactions among fermions the particle-hole pairs cannot scatter-off each other so the decay of the bosons is limited to the single-pair continuum. In the high-frequency regime the self-energy part Eq. (27) and the DSF Eq. (30) are smooth functions of frequency and momentum. These results are valid to all orders in interactions but only in second-order in curvature, *i.e.* the 2-pair continuum. As a consequence, this second-order contribution is the leading contribution with respect to the high-frequency part of the dynamic structure factor of one-dimensional fermions Eq. (30). The nonlinear bosonization technique therefore works away from the plasmon-cone even though it is limited to a perturbative result in curvature.

On the other hand the second-order low-frequency result, Eq. (29), is singular (it's imaginary part from which the structure factor is defined). This implies that curvature is unable to cure the bosonization technique from its singularities order by order. Reciprocally, bosonization, being limited to a perturbative evaluation of band-curvature effects, is unable to resolve the two-parametric family of Eq. (5) starting from the single-parametric one, $\omega = u_\rho|q|$. This was already the case for free fermions, Eq. (7), where an infinite number of terms had to be evaluated and summed in order for the DSF to be well-defined at low frequencies, see Eq. (10). In the free-fermion case an exact solution was available to overcome the singular perturbation theory. In the presence of interactions and within bosonization no such solution is available, to our knowledge, and we face a tedious order by order calculation. In the φ -representation the fourth order diagrams are displayed on Fig. 6.

III. SPINFUL FERMIONS

A. Model

Following the previous sections we now move to spinful fermions by introducing an additional internal, spin-1/2, degree of freedom to the fields: $\sigma = \uparrow, \downarrow$, so that:

$$\begin{aligned} \psi_{\pm, \sigma}(x) &= \frac{1}{\sqrt{2\pi}} : \exp \left[\pm i \sqrt{4\pi} \varphi_{\pm, \sigma}(x) \right] :, \\ \varphi_{\pm, \sigma} &= \frac{1}{2} \left(\varphi_\sigma \mp \int_{-\infty}^x dx' \Pi_\sigma(x') \right). \end{aligned}$$

This yields:

$$\begin{aligned} H &= v \sum_{\sigma} \int dx \left[(\partial_x \varphi_{+, \sigma})^2 + (\partial_x \varphi_{-, \sigma})^2 \right] \\ &\quad - \frac{2\sqrt{\pi}}{3m} \int dx \left[(\partial_x \varphi_{+, \sigma})^3 + (\partial_x \varphi_{-, \sigma})^3 \right], \end{aligned}$$

with the densities:

$$\rho_{\eta, \sigma}(x) = -\frac{1}{\sqrt{\pi}} \partial_x \varphi_{\eta, \sigma}(x).$$

We then introduce the charge and spin fields together with their canonically conjugated fields:

$$\begin{aligned} \varphi &= \frac{1}{\sqrt{2}} [\varphi_{\uparrow} + \varphi_{\downarrow}], & \sigma &= \frac{1}{\sqrt{2}} [\varphi_{\uparrow} - \varphi_{\downarrow}], \\ \Pi_{\varphi} &= \frac{1}{\sqrt{2}} [\Pi_{\uparrow} + \Pi_{\downarrow}], & \Pi_{\sigma} &= \frac{1}{\sqrt{2}} [\Pi_{\uparrow} - \Pi_{\downarrow}]. \end{aligned}$$

The Hamiltonian density then takes the following form:

$$\mathcal{H} = \mathcal{H}_{TL} + \mathcal{H}_C, \quad (31a)$$

$$\begin{aligned} \mathcal{H}_{TL} &= \frac{u_\rho}{2} \left[\gamma_\rho \Pi_\varphi^2 + \frac{1}{\gamma_\rho} (\partial_x \varphi)^2 \right] + \\ &\quad + \frac{u_\sigma}{2} \left[\gamma_\sigma \Pi_\sigma^2 + \frac{1}{\gamma_\sigma} (\partial_x \sigma)^2 \right], \end{aligned} \quad (31b)$$

$$\begin{aligned} \mathcal{H}_C &= -\frac{1}{m'} \left[(\partial_x \varphi)^3 + 3 \partial_x \varphi \Pi_\varphi^2 + \right. \\ &\quad \left. + 3 \partial_x \sigma [(\partial_x \sigma)^2 + \Pi_\sigma^2] + 6 \Pi_\varphi \partial_x \sigma \Pi_\sigma \right], \end{aligned} \quad (31c)$$

where $m' = 6m/\sqrt{\pi}$. In Eqs. (31) interactions in the charge and spin sectors have been included. For the latter we have introduced the following parameters:

$$\begin{aligned} \gamma_\sigma &= \sqrt{\frac{1 + g_{4,s}/2 - g_{2,s}/2}{1 + g_{4,s}/2 + g_{2,s}/2}}, \\ u_\sigma &= v \sqrt{(1 + g_{4,s}/2)^2 - (g_{2,s}/2)^2}, \end{aligned}$$

where $g_{i,s} \equiv g_{i,s}/\pi v$ is the dimensionless coupling constant in the spin sector. Just as for the charge sector in the following we take: $g_{2,s} = g_{4,s} = g_s$, which yields:

$$\gamma_\sigma = \frac{1}{\sqrt{1 + g_s}} (= 1), \quad u_\sigma = v \sqrt{1 + g_s} (= v). \quad (32)$$

In the absence of curvature ($m' \rightarrow \infty$) only Eq. (31b) remains which corresponds to the usual Tomonaga-Luttinger model. It's main feature is the separation of the Hilbert spaces associated with charge and spin sectors (the spin and charge parts commute with each-other; recall the anomalous commutations: $[\varphi(x), \Pi_\varphi(x')] = i\delta(x - x')$, and similarly for σ and Π_σ , while other commutators are zero). Moreover, as can be seen from:

$$\rho_\rho(x) = -\sqrt{\frac{2}{\pi}} \partial_x \varphi, \quad \rho_\sigma(x) = -\sqrt{\frac{2}{\pi}} \partial_x \sigma, \quad (33)$$

$$j_\rho(x) = \sqrt{\frac{2}{\pi}} \partial_t \varphi, \quad j_\sigma(x) = \sqrt{\frac{2}{\pi}} \partial_t \sigma,$$

kinks in φ determine the density of fermions while, independently, kinks in σ determine the magnetization density due to the spin of these fermions (we are considering the smooth part of the densities close to $q = 0$; the $q = 2k_F$ parts are neglected). Charge and spin travel at different velocities: u_ρ and u_σ , respectively, which are determined by the interactions among the fermions. As a result, charge flies away from spin so that the interacting fermions decompose into two elementary excitations. These are the spinless charged holon and anti-holon and the chargeless spin-1/2 spinon, see the textbooks [5,6]. The Gaussian nature of the TL model implies that these excitations are free.

In the presence of curvature the elementary excitations acquire a finite lifetime. In particular, the first two terms in Eq. (31c) are identical to the ones found in the spinless case and lead to the decay of the charge excitations within the charge sector. More importantly, the next terms in Eq. (31c) show that spin and charge Hilbert spaces are no more decoupled when curvature is introduced. As we know from the exact solution of the Hubbard model, *e.g.* Refs. [8,9] for reviews, the decoupling still exists at the level of the elementary excitations²²: holons and spinons, but the latter interact with each other. This opens new channels for the decay of the excitations²³. Indeed, the third and fourth terms couple the charge density to the spin density and current, respectively. And the last term describes the coupling between the charge and spin currents. Moreover, we see from Eq. (31c) that spin and charge degrees of freedom do not enter in a symmetric way. As a matter of fact, the decay of spin excitations can only take place by affecting the whole charge density along the wire.

Even though we have derived Eq. (31) the general form of the Hamiltonian and the particular asymmetry between spin and charge may be understood from general symmetry considerations. This allows a phenomenological approach to the model. As in the spinless case, the fact that all curvature terms are cubic is related to the energy of the Fermi sea for a quadratic single-particle spectrum. It implies that the particle-hole symmetry is violated which is natural away from half-filling for such a spectrum. Moreover, the curvature terms in Eq. (31c), are compatible with the basic symmetries of the problem: φ and σ are odd functions of x and even functions

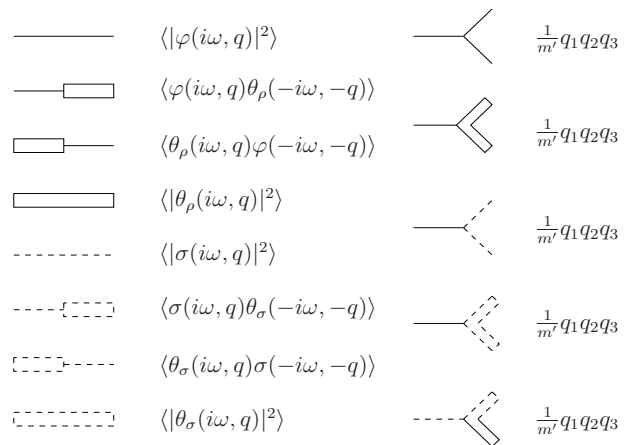


FIG. 7: The quantum field theory associated with the Lagrangian of Eq. (34) for spinful fermions.

of t , see Eqs. (33). Finally, Eq. (31c) is invariant under $U(1)$ transformations of the charge fields and $SU(2)$ transformations of the spin fields. The latter is not quite explicit here since we are using the Abelian bosonization technique²⁵. Nevertheless, as a weak manifestation of the $SU(2)_1$ symmetry, all spin-fields in Eq. (31c) are paired, *e.g.* a term of the form $\partial_x \varphi \Pi_\varphi \Pi_\sigma$ is compatible with the basic symmetries but is not $SU(2)$ invariant. Another consequence of the $SU(2)$ spin-rotational invariance of the theory, *e.g.* see [6], is that $g_s = -g_1/2$ where g_1 is the dimensionless coupling constant arising from backscattering. Thus, from Eq. (32) and in the absence of backscattering, the spin parameters are the free ones: $u_\sigma = v$ and $\gamma_\sigma = 1$. We will work with general values of these parameters in what follows and set them to their non-interacting value at the end of the calculations.

To proceed further, we go to the Lagrangian formulation by introducing the dual fields: θ_ρ and θ_σ , such that: $\Pi_\varphi = \partial_x \theta_\rho$ and $\Pi_\sigma = \partial_x \theta_\sigma$. This yields:

$$\begin{aligned} \mathcal{L}_E[\varphi, \sigma; \theta_\rho, \theta_\sigma] = & \\ & \frac{u_\rho \gamma_\rho}{2} (\partial_x \theta_\rho)^2 + \frac{u_\rho}{2\gamma_\rho} (\partial_x \varphi)^2 - i \partial_x \theta_\rho \partial_\tau \varphi \\ & + \frac{u_\sigma \gamma_\sigma}{2} (\partial_x \theta_\sigma)^2 + \frac{u_\sigma}{2\gamma_\sigma} (\partial_x \sigma)^2 - i \partial_x \theta_\sigma \partial_\tau \sigma \\ & - \frac{1}{m'} \partial_x \varphi [(\partial_x \varphi)^2 + 3(\partial_x \theta_\rho)^2] \\ & - \frac{3}{m'} \partial_x \varphi [(\partial_x \sigma)^2 + (\partial_x \theta_\sigma)^2] \\ & - \frac{6}{m'} \partial_x \theta_\rho \partial_x \sigma \partial_x \theta_\sigma. \end{aligned} \quad (34)$$

The field theory associated with Eq. (34) is defined in Fig.7. In the charge sector, bare correlators are given by Eqs. (26) with $\theta \equiv \theta_\rho$. Following the spinless case the correlator $\mathcal{D}_\varphi^{(0)}$ is associated with the particle-hole pair excitations. These are *charge-neutral* excitations, even though we will often refer to them as charge excitations,

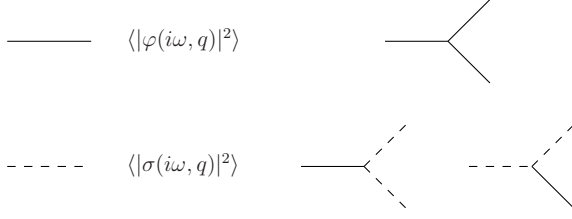


FIG. 8: The quantum field theory related to the Lagrangian of Eq. (36) for spinful fermions.

for simplicity, as holons and anti-holons never appear explicitly²³. Moreover, as there is no spin-charge coupling at the level of the bare propagators, these charge-neutral excitations are spinless. In the spin sector, the bare correlators read:

$$\begin{aligned}
 \mathcal{D}_{\sigma\sigma}^{(0)}(i\omega, q) &= \langle |\sigma(i\omega, q)|^2 \rangle = -\frac{u_\sigma \gamma_\sigma}{(i\omega)^2 - (u_\sigma q)^2}, \\
 \mathcal{D}_{\theta_\sigma \theta_\sigma}^{(0)}(i\omega, q) &= \langle |\theta_\sigma(i\omega, q)|^2 \rangle = -\frac{u_\sigma}{\gamma_\sigma} \frac{1}{(i\omega)^2 - (u_\sigma q)^2}, \\
 \mathcal{D}_{\sigma\theta_\sigma}^{(0)}(i\omega, q) &= \langle \sigma(i\omega, q) \theta_\sigma(-i\omega, -q) \rangle = \frac{-i\omega}{q[(i\omega)^2 - (u_\sigma q)^2]}, \\
 \mathcal{D}_{\theta_\sigma \sigma}^{(0)}(i\omega, q) &= \mathcal{D}_{\sigma\theta_\sigma}^{(0)}(i\omega, q),
 \end{aligned} \tag{35}$$

where $\mathcal{D}_{\sigma\sigma}^{(0)}$ is associated with spin-singlet or triplet excitations. We shall often refer to them as spin excitations, for simplicity, as spinons never appear explicitly²³. They are chargeless.

Alternatively, we may also integrate over the dual fields in Eq. (34) and work with the following reduced Lagrangian:

$$\begin{aligned}
 \mathcal{L}_E[\varphi, \sigma] &= \frac{1}{2\gamma_\rho} \left[\frac{1}{u_\rho} (\partial_\tau \varphi)^2 + u_\rho (\partial_x \varphi)^2 \right] \\
 &+ \frac{1}{2\gamma_\sigma} \left[\frac{1}{u_\sigma} (\partial_\tau \sigma)^2 + u_\sigma (\partial_x \sigma)^2 \right] \\
 &+ \frac{1}{m'v^2} \partial_x \varphi \left[3(\partial_\tau \varphi)^2 - v^2 (\partial_x \varphi)^2 \right] \\
 &+ \frac{3}{m'v^2} \partial_x \varphi \left[(\partial_\tau \sigma)^2 - v^2 (\partial_x \sigma)^2 \right] \\
 &+ \frac{6}{m'v^2} \partial_\tau \varphi \partial_x \sigma \partial_\tau \sigma,
 \end{aligned} \tag{36}$$

where only the lowest order terms in $1/m'$ have been taken into account. The corresponding field theory is given on Fig. 8.

With the help of the models of Eqs. (34) and (36), we will determine the effects of the spin-charge mixing terms arising from band-curvature on the response functions of the system at small wave-vector q . There are two of them: the charge DSF and the spin (or magnetic) DSF (mixed correlators of the type: $\langle \varphi(i\omega, q) \sigma(-i\omega, -q) \rangle$), are zero within the present field theory because there is no spin-charge mixing at the level of the bare propagators).



FIG. 9: Second-order diagrams contributing to the charge density correlation function generated from the φ, σ -Lagrangian of Eq. (36) for spinful fermions.

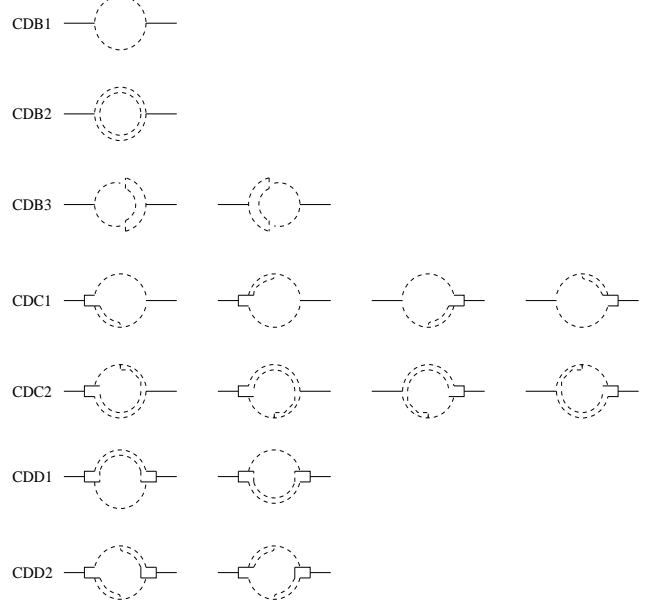


FIG. 10: Second-order diagrams mixing spin and charge degrees of freedom and contributing to the charge density correlation function of spinful fermions. These diagrams are generated with the $\varphi, \sigma, \theta_\rho, \theta_\sigma$ -Lagrangian of Eq. (34). The self-energy parts only depend on the spin degrees of freedom. CD stands for Charge Density. The set CDA is identical to the diagrams appearing in the spinless case, Fig. 5, and is not displayed. The sets CDB, CDC and CDD are analyzed in Appendix D 1. Notice that, up to the fact that the self-energy depends only on the spin degrees of freedom, these diagrams are the same as those of the spinless case, Fig. 5.

B. Dynamical charge structure factor

We first compute the second-order corrections in band-curvature to the charge DSF of spinful fermions. They correspond to the diagrams of Fig. 9 in the φ, σ -representation. The latter include a contribution which is similar to the spinless case, the first diagram in Fig. 9, arising from the decay of a charge (-neutral) boson into two charge (-neutral) bosons, see the first vertex in Fig. 8. Because of band curvature, spin-charge separation is violated and spin degrees of freedom provide another channel for the decay of the charge boson. This channel corresponds to the second vertex of Fig. 8 whereby the charge boson decays into two spin bosons (each corresponding to a spin-singlet excitation). The corresponding, second-order in band-curvature, diagram is the second diagram of Fig. 9.

In the $\varphi, \sigma, \theta_\rho, \theta_\sigma$ -representation of Eq. (34) the new

diagram is given by the diagrams of Fig. 10 where the same classification as in the spinless case, Fig. 5, has been used, *i.e.* diagrams are classified according to the number of θ -wings attached to their self-energy parts, see Appendices C 2 and D 1. The increased number of diagrams in Fig. 10 with respect to Fig. 9 reflects the non-trivial nature of the vertices of the cubic field theory under consideration.

The diagrams of Figs. 9 and 10 have the same structure as those of the corresponding spinless case, Figs. 3 and 5, respectively. In the case where charge and spin parameters are equal ($\gamma_\rho = \gamma_\sigma = \gamma$ and $u_\rho = u_\sigma = u$), the free-fermion case being a special sub-case ($\gamma = 1$ and $u = v$), the diagrams of Fig. 9 reduce to the one of Fig. 3 with an additional factor of 2, the spin degeneracy. Similarly, the diagrams of Fig. 10 add with those of Fig. 5 and yield an overall factor of 2. To appreciate the spin-charge coupling one has therefore to impose an inequivalence between these degrees of freedom.

This arises naturally by switching on interactions in the charge sector because the spin sector is free as there is no backscattering, see Eq. (32) and discussion below it. For arbitrary values of these parameters, following the calculations of Appendix D 1, the total self-energy, close to $q = 0$, of interacting spinful fermions reads (at $T = 0$):

$$\begin{aligned} \Im\Sigma_\rho^R(\omega, q) &= \frac{\pi}{96} \left(\frac{q^2}{m}\right)^2 \quad (37) \\ &\left[\frac{\gamma_\rho^2}{u_\rho} \left[1 + \frac{3}{\gamma_\rho^2}\right]^2 u_\rho q [\delta[\omega - u_\rho q] - \delta[\omega + u_\rho q]] \right. \\ &+ \left. \frac{\gamma_\sigma^2}{u_\sigma} \left[1 + \frac{1}{\gamma_\sigma^2} + \frac{2}{\gamma_\sigma \gamma_\rho}\right]^2 u_\sigma q [\delta[\omega - u_\sigma q] - \delta[\omega + u_\sigma q]] \right] \\ &+ \frac{\gamma_\rho^2 \pi}{64u_\rho} \left[1 - \frac{1}{\gamma_\rho^2}\right]^2 \left(\frac{q}{mu_\rho}\right)^2 [\omega^2 - (u_\rho q)^2] \mathcal{F}_\rho(\omega, q) \\ &+ \frac{\gamma_\sigma^2 \pi}{64u_\sigma} \left[1 - \frac{1}{\gamma_\sigma^2}\right]^2 \left(\frac{q}{mu_\sigma}\right)^2 [\omega^2 - (u_\sigma q)^2] \mathcal{F}_\sigma(\omega, q), \end{aligned}$$

where the kinematic factor reads:

$$\mathcal{F}_\sigma(\omega, q) = \theta[\omega - u_\sigma q] - \theta[-\omega - u_\sigma q]. \quad (38)$$

This general result shows that the density correlation function of spinful fermions has two peaks: a charge peak at $\omega = u_\rho q$ but also a spin peak at $\omega = u_\sigma q$ so that part of the charge spectral weight is carried by the spin-singlet. Each peak has tails due to the interactions between the fermions composing the bosonic excitations during the decay process. In the absence of backscattering, *i.e.* for $\gamma_\sigma = 1$ and $u_\sigma = v$, spin excitations are free so that the 2-pair tail related to their scattering disappears from

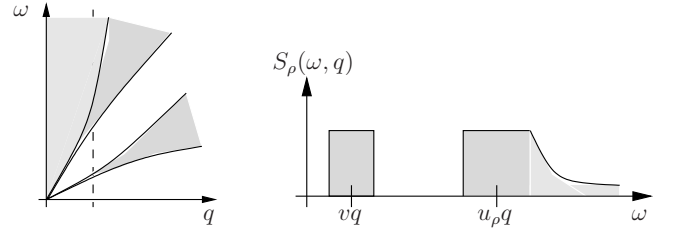


FIG. 11: Schematic view on the low-momentum ($q \ll k_F$) part of the spectrum of excitation of spinful fermions and the corresponding charge DSF. Interactions are present in the charge sector ($\gamma_\rho < 1$) while the spin sector is free ($\gamma_\sigma = 1$). Because of the violation of spin-charge separation due to band-curvature two branches appear. The higher one corresponds to the usual charge branch and has a high-frequency tail (displayed in light gray). The lower one is the spin branch and has no frequency tail. Along the cut a two-peak structure for the corresponding charge DSF is revealed.

Eq. (37). The latter then simplifies as:

$$\begin{aligned} \Im\Sigma_\rho^R(\omega, q) &= \quad (39) \\ &\frac{\gamma_\rho^2 \pi}{96u_\rho} \left[1 + \frac{3}{\gamma_\rho^2}\right]^2 \left(\frac{q^2}{m}\right)^2 u_\rho q [\delta[\omega - u_\rho q] - \delta[\omega + u_\rho q]] \\ &+ \frac{\pi}{24v} \left[1 + \frac{1}{\gamma_\rho}\right]^2 \left(\frac{q^2}{m}\right)^2 vq [\delta[\omega - vq] - \delta[\omega + vq]] \\ &+ \frac{\gamma_\rho^2 \pi}{64u_\rho} \left[1 - \frac{1}{\gamma_\rho^2}\right]^2 \left(\frac{q}{mu_\rho}\right)^2 [\omega^2 - (u_\rho q)^2] \mathcal{F}_\rho(\omega, q). \end{aligned}$$

The spin-charge mixing, which is responsible for the appearance of the spin peak in the above self-energy, is even more apparent from the pole structure of the corresponding correction to the polarization operator:

$$\begin{aligned} \Pi^{(2)}(i\omega, q) &= \frac{\gamma_\rho^2}{12\pi} \left(\frac{q^2}{m}\right)^2 \quad (40) \\ &\left[\frac{\gamma_\rho^2}{4u_\rho} \left[1 + \frac{3}{\gamma_\rho^2}\right]^2 \frac{(u_\rho q)^4}{[(i\omega)^2 - (u_\rho q)^2]^3} \right. \\ &+ \left. \frac{1}{v} \left[1 + \frac{1}{\gamma_\rho}\right]^2 \frac{(vq)^2 (u_\rho q)^2}{[(i\omega)^2 - (vq)^2][(i\omega)^2 - (u_\rho q)^2]^2} \right], \end{aligned}$$

where the high-frequency part has been neglected. In Eq. (40) the second term mixes spin and charge, gives rise to the spin peak and renormalizes the effective band-mass of the charge peak. Moreover, the spin peak at $\omega = v|q|$ has no long-range tails and in the limit of strong repulsive interactions, $\gamma_\rho \ll 1$, is well separated from the charge peak at $\omega = u_\rho|q| = v|q|/\gamma_\rho \gg v|q|$. The latter has long-range tails given by Eq. (30).

The additional spin peak to the DSF is a witness of the spin-charge coupling due to band-curvature. It arises from the opening of a new channel for the decay of charge (-neutral) excitations, *i.e.* into two gapless spin-singlets traveling at $u_\sigma = v < u_\rho$. The sharpness of this spin

peak translates the coherence of the rearrangement of the background charge²⁴ due to the spin-singlet. However, the 2-parametric nature of the excitations, *i.e.* the widths of the spin and charge peaks which are schematically displayed on Fig. 11, cannot be accessed by the present second-order perturbation theory in curvature, see related discussion in Sec. II C.

C. Dynamical spin structure factor

We now focus on the spin degrees of freedom. The long-distance part (close to $q = 0$; the $2k_F$ -part is neglected) of the spin-density correlation function is defined as:

$$\chi(x, \tau) = \frac{1}{\pi} \langle \partial_x \sigma(x, \tau) \partial_x \sigma(0, 0) \rangle, \quad (41)$$

and, in Fourier space, reads:

$$\chi(i\omega, q) = -\frac{q^2}{\pi} \mathcal{D}_{\sigma\sigma}(i\omega, q). \quad (42)$$

The dynamic spin structure factor corresponds to the dissipative part of this susceptibility:

$$S_\sigma(\omega, q) = -\Im \chi^R(\omega, q). \quad (43)$$

In the absence of curvature the result is well known:

$$S_\sigma^0(\omega, q) = \frac{\gamma_\sigma}{u_\sigma} (u_\sigma q)^2 \delta[\omega^2 - (u_\sigma q)^2], \quad (44)$$

with obvious similarity with the dynamical charge structure factor.

Including curvature, the second-order correction to the spin density correlation function reads:

$$\chi^{(2)}(i\omega, q) = -\frac{\gamma_\sigma^2}{\pi} \frac{(u_\sigma q)^2}{[(i\omega)^2 - (u_\sigma q)^2]^2} \Sigma_\sigma(i\omega, q), \quad (45)$$

where the self-energy Σ_σ is given by the diagrams of Fig. 12 in the the φ, σ -representation of Lagrangian Eq. (36). These diagrams are built from the third vertex displayed on Fig. 8 which shows that a spin excitation (singlet, triplet) can decay only into a mixed spin (singlet, triplet, resp.) – charge-neutral excitation. Contrary to charge fluctuations which had two-channels through which they could decay (one of them not affecting the spin degrees of freedom and therefore surviving in the spinless case) the decay of spin fluctuations cannot proceed without affecting the whole charge background.

In the $\varphi, \sigma, \theta_\rho, \theta_\sigma$ -representation of Lagrangian Eq. (34), which reveals the non-trivial nature of the vertices of the cubic field theory, these mixed spin-charge self-energy parts are displayed on Fig. 13.

In the case where spin and charge degrees of freedom are equivalent ($\gamma_\rho = \gamma_\sigma = \gamma$ and $u_\rho = u_\sigma = u$), the free-fermion case being a special sub-case ($\gamma = 1$ and $u = v$), spin and charge bare propagators are equal so that there



FIG. 12: Second-order diagrams contributing to the spin-density correlation function and generated from the φ, σ -Lagrangian of Eq. (36) for spinful fermions.

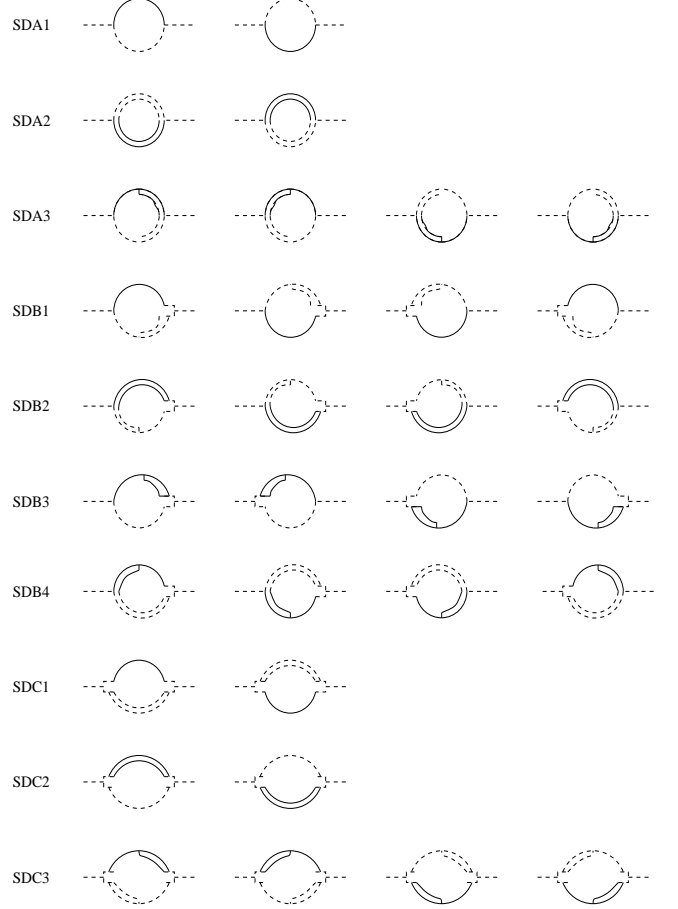


FIG. 13: Second-order diagrams contributing to the spin-density correlation function and generated from the $\varphi, \sigma, \theta_\rho, \theta_\sigma$ -Lagrangian of Eq. (34) for spinful fermions. All the self-energy parts mix spin and charge and are analyzed in Appendix D 2. SD stands for Spin Density. In the limit where spin and charge degrees of freedom are equal these diagrams reduce to those of Fig. 5 up to spin degeneracy.

is no more difference between the solid and dashed lines in Figs. 12 and 13. One can then easily check that in this case the diagrams of Figs. 12 and 13 are identical to those of Figs. 3 and 5, respectively, with an additional factor of 2 due to the spin degeneracy.

All non-trivial effects that we shall observe below are therefore related to the fact that spin and charge excitations travel at different velocities. This imbalance is naturally achieved by switching on interactions in the charge sector as the spin sector is free because fermions do not backscatter off each-other. In Appendix D 2 we provide the reader with some of the details of the calcula-

tion for general values of the charge and spin parameters, see Eq. (D6). Switching off the backscattering ($\gamma_\sigma = 1$ and $u_\sigma = v$) this equation simplifies as (at $T = 0$ for simplicity):

$$\begin{aligned} \Im \Sigma_\sigma^R(\omega, q) = & \quad (46) \\ & \frac{\gamma_\rho \pi}{8v} \left[1 + \frac{1}{\gamma_\rho}\right]^2 \left[1 + \frac{\omega}{vq}\right]^2 \left(\frac{q^2}{m}\right)^2 vq \\ & \frac{[\omega - vq][\omega - u_\rho q]}{|u_\rho - v|^3 q^3} \left[\theta \left[-\frac{u_\rho[\omega - vq]}{u_\rho - v} \right] - \theta \left[-\frac{v[\omega - u_\rho q]}{u_\rho - v} \right] \right] \\ & + \frac{\gamma_\rho \pi}{8v} \left[1 + \frac{1}{\gamma_\rho}\right]^2 \left[1 - \frac{\omega}{vq}\right]^2 \left(\frac{q^2}{m}\right)^2 vq \\ & \frac{[\omega + vq][\omega + u_\rho q]}{|u_\rho - v|^3 q^3} \left[\theta \left[-\frac{u_\rho[\omega + vq]}{u_\rho - v} \right] - \theta \left[-\frac{v[\omega + u_\rho q]}{u_\rho - v} \right] \right] \\ & + \frac{\gamma_\rho \pi}{8} \left[1 - \frac{1}{\gamma_\rho}\right]^2 \left[1 - \frac{\omega}{vq}\right]^2 \left(\frac{q}{m}\right)^2 \frac{1}{|u_\rho + v|^3} \\ & [\omega + vq][\omega - u_\rho q] \left[\theta \left[\frac{v[\omega - u_\rho q]}{u_\rho + v} \right] - \theta \left[-\frac{u_\rho[\omega + vq]}{u_\rho + v} \right] \right] \\ & + \frac{\gamma_\rho \pi}{8} \left[1 - \frac{1}{\gamma_\rho}\right]^2 \left[1 + \frac{\omega}{vq}\right]^2 \left(\frac{q}{m}\right)^2 \frac{1}{|u_\rho + v|^3} \\ & [\omega - vq][\omega + u_\rho q] \left[\theta \left[\frac{v[\omega + u_\rho q]}{u_\rho + v} \right] - \theta \left[-\frac{u_\rho[\omega - vq]}{u_\rho + v} \right] \right]. \end{aligned}$$

Notice that in the limit where $\gamma_\rho \rightarrow 1$ in Eq. (46) the first two terms become δ -functions centered around $\pm vq$ and the last two terms vanish. This yields back Eq. (44) for the magnetic DSF. On the other hand for $\gamma_\rho < 1$ second-order curvature effects broaden the peaks at $\pm vq$ by transferring spectral weight to frequencies reaching the charge frequency ($u_\rho q$) with additional long-range tails. This is more conveniently seen on the magnetic DSF. The latter is non-zero all the way between the spin and charge frequencies:

$$\begin{aligned} S_\sigma^{(2)}(\omega, q) = & \frac{\gamma_\rho}{8v} \left(\frac{q}{mv}\right)^2 [\theta[-\omega + u_\rho q] - \theta[-\omega + vq]] \\ & \left[\frac{[1/\gamma_\rho + 1]^2}{|1/\gamma_\rho - 1|^3} \frac{\omega - u_\rho q}{\omega - vq} + \frac{[1/\gamma_\rho - 1]^2}{|1/\gamma_\rho + 1|^3} \frac{\omega + u_\rho q}{\omega - vq} \right], \quad (47) \end{aligned}$$

where, for simplicity, we have set $q > 0$ and focused on $\omega > vq$.

At $\omega = vq$ this expression diverges but only algebraically and not as a δ -function as for the zero-order term or in the absence of interactions.

At $\omega = u_\rho q$ the magnetic DSF is finite and equals:

$$S_\sigma^{(2)}(u_\rho q, q) = \frac{1}{4v} \frac{1/\gamma_\rho - 1}{|1/\gamma_\rho + 1|^3} \left(\frac{q}{mv}\right)^2, \quad (48)$$

so that part of the magnetic spectral weight is carried by the charge excitations.

At large frequencies, $\omega \gg u_\rho q$, tails appear and read:

$$\begin{aligned} S_\sigma^{(2)}(\omega, q) = & \frac{\gamma_\rho}{4v} \left[\frac{1/\gamma_\rho - 1}{|1/\gamma_\rho + 1|} \right]^2 \left(\frac{q^2}{m}\right)^2 \frac{\theta[\omega - u_\rho q]}{\omega^2 - (vq)^2} \\ & + \frac{\gamma_\rho}{4v} \frac{[1/\gamma_\rho - 1]^2}{|1/\gamma_\rho + 1|^3} \left(\frac{q}{mv}\right)^2 \theta[\omega - u_\rho q]. \quad (49) \end{aligned}$$

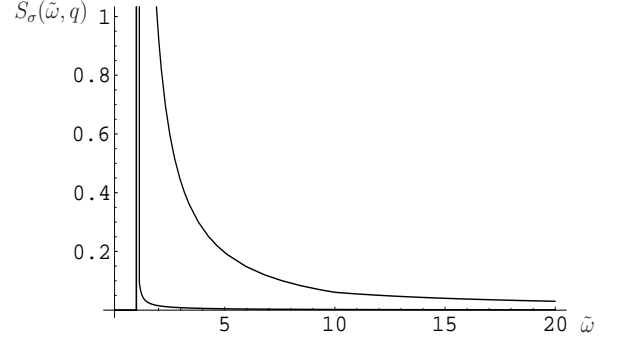


FIG. 14: The magnetic structure factor, $S_\sigma(\tilde{\omega}, q)$, at a fixed q , as a function of the dimensionless frequency $\tilde{\omega} = \omega/vq$ and for different interaction strengths in the charge sector ($\gamma_\sigma = 1$). This figure shows a transfer of the spectral weight to higher frequencies as the interaction strength increases. This transfer originates from the spin-charge coupling due to band-curvature. The spectral weight then extends from the spin excitation frequency, $\tilde{\omega}_\sigma = 1$, to the interaction-dependent charge excitation frequency, $\tilde{\omega}_\rho = 1/\gamma_\rho$, with additional high frequency tails. The peak at $\tilde{\omega} = 1$ corresponds to the free fermion result: $\gamma_\rho = 1$ ($\tilde{\omega}_\sigma = \tilde{\omega}_\rho = 1$). The second curve corresponds to the second-order curvature correction at $\gamma_\rho = 0.9$ ($\tilde{\omega}_\rho = 1.1$). The third curve corresponds to the second-order curvature correction at $\gamma_\rho = 0.1$ ($\tilde{\omega}_\rho = 10$).

Notice that the second term in Eq. (49) yields a non-zero dissipation at infinite frequencies. Nevertheless, the spin-structure factor satisfies the sum-rule:

$$\int_0^\infty d\omega \omega S_\sigma(\omega, q) = \frac{v^* q^2}{2}, \quad (50)$$

but with a re-normalized spin-velocity, v^* , which reads:

$$\frac{v^*}{v} = 1 + \frac{\gamma_\rho^2}{4} \frac{[1 - \gamma_\rho]^2}{|1 + \gamma_\rho|^3}, \quad v < v^* < u_\rho. \quad (51)$$

In Eq. (50) a large frequency cut-off at $\epsilon_F = mv^2$ has been included and the final result was obtained after sending this cut-off to infinity. The re-normalization of the spin-velocity by interactions in the charge sector is precisely due to the last term in Eq. (49). It is a signature that the physical excitations carrying the magnetic spectral weight, in the tails of the spin-structure factor, are spin (-singlet or -triplet) excitations dressed by charge-neutral ones.

We therefore see that band-curvature softens the singularities of the spin structure factor already at the second order of perturbation theory. Such an effect arises from spin-charge mixing and is more dramatic than for the charge DSF. The latter was also affected by the violation of the spin-charge separation due to band curvature (*cf.* the double peak structure, see Eqs. (39) and (40) and Fig. 11) but its low frequency part was still δ -singular at second order in band-curvature. The sharpness of both charge and spin peaks in the charge DSF was due to the

decay of charge fluctuations into either a pair of charge-neutral excitations or a pair of spin-singlet excitations, both coherently traveling at velocities u_ρ and u_σ , respectively. On the other hand spin fluctuations decay via spin(-singlet or -triplet) – charge(-neutral) excitations. Both components of this pair lead to rearrangement of the background charge along the wire²⁴. But they travel at different velocities. As a consequence, the redistribution of magnetic spectral weight is incoherent and affects an infinite number of modes. The magnetic DSF is plotted on Fig. 14 for different values of the interactions in the charge sector. Because of the spin-charge coupling just described more spectral weight is transferred from the spin peak at $\omega = vq$ to the charge peak at $\omega = u_\rho q = vq/\gamma_\rho$, upon increasing interactions.

IV. CONCLUSION

Using the (Abelian) bosonization technique we have studied the charge and spin equilibrium dynamics of 1D fermions in clean quantum wires with forward scattering interactions, *i.e.* below half-filling, and quadratic band-curvature corrections to the linear single-particle spectrum, *cf.* Eq. (3). The dynamics were accessed by calculating the charge and magnetic dynamical structure factors at small wave-vector q . They may be measured experimentally with the help of electron energy-loss spectroscopy and neutron scattering, respectively. The introduction of band-curvature corrections allowed us to explore the high-energy physics of fermions in quantum wires. This is a basic step beyond the standard Tomonaga-Luttinger model which assumes a linear dispersion, Eq. (1). In solid-state physics this relativistic approximation is valid only at low-energies. It is also a basic step towards the Hubbard model (below half-filling) which has the full non-linear spectrum of lattice fermions, Eq. (2). The main features which were analyzed are the multi-pair excitation continuum to the DSF, *cf.* Sec. II, and the spin-charge coupling, *cf.* Sec. III. Both are absent in the low-energy sector of the theory (spin-charge separation being one of the most distinguished features of the TL liquid) and both result from the interplay between band-curvature and interactions in the charge sector. The calculations were carried out with the help of the bosonization technique. This is a standard low-energy Lorentz invariant field-theory technique. Nevertheless, we have extended it to include band-curvature, *i.e.* made the bosonization non-linear. This allowed us to access some of the limitations of this standard technique close to the frequency of the elementary excitations of the system as well as its efficiency at higher frequencies.

In Sec. II the case of spinless fermions has been analyzed with the help of the two model Lagrangians of Eqs. (22) and (23). We have derived these Lagrangians, following earlier works [4,14,20], but their form maybe understood on a phenomenological basis. The curvature terms are cubic in the charge currents which is related

to the energy of the Fermi sea for a quadratic spectrum. They translate the violation of the particle-hole symmetry away from half-filling. Space-time symmetries as well as the $U(1)$ symmetry of the charge field then fully determine the allowed combinations of currents composing the cubic terms. The non-Gaussian nature of the models is a signature of the interactions between the elementary bosonic excitations. We then proceeded to study their equilibrium dynamics by calculating the DSF of the model perturbatively in band-curvature. The φ -Lagrangian of Eq. (22) and the φ, θ -Lagrangian of Eq. (23) are equivalent at second-order. The decay of the Bose excitations is best revealed in the φ -representation while the φ, θ -representation displays the non-trivial nature of the cubic field theory, *cf.* Fig. 4. The corresponding diagrams for the DSF were given on Figs. 3 and 5, respectively. Our main result is Eq. (27) for the self-energy part of the DSF, in second-order in band-curvature and to all orders in interactions. At small frequencies, *i.e.* close to the plasmon-cone $\omega = u_\rho|q|$, this self-energy part and the corresponding correction to the polarization operator Eq. (29) are δ -singular. The latter is equal to the corresponding correction in the free-fermion case up to a re-normalization of the band-mass and the velocity of the excitations by interactions. To overcome the singularity of the perturbation in band-curvature an infinite number of terms have to be evaluated and summed. Some of them are represented on Fig. 6. This summation would enable us to determine the 2-parametric spectrum of the excitations together with the precise spectral line-shape of the DSF. The difficulty to achieve this task is a witness of the limitation of the bosonization technique. It justifies alternative routes to deal with the plasmon-cone such as fermionic approaches, *cf.* Ref. [18,19], or numerical methods, *cf.* [20]. On the other hand at high frequencies, *i.e.* away from the cone $\omega \gg u_\rho|q|$, Eq. (27) shows that, in the presence of interactions, the self-energy is non-zero and a smooth function of frequency and momentum. This manifests as high-frequency tails in the DSF, Eq. (30) and Fig. 2. As already known from Ref. [20] the bosonization technique therefore efficiently describes the 2-pair excitation continuum whereby a coherent excitation decays by emitting two particle-hole pairs. At such high frequencies, where a perturbative treatment of band-curvature is justified, bosonization is as efficient as fermionic approaches, *cf.* [15,21].

In Sec. III we proceeded further by including an internal, spin-1/2, degree of freedom to the fermions. In the TL model, a spinful fermion is known to decompose into a spinless charged holon or anti-holon and a chargeless spin-1/2 spinon. In the linear spectrum approximation they are free elementary excitations. In the presence of curvature the spin-charge decoupling is still present at the level of these elementary excitations²². However, the latter interact with each-other which couples their Hilbert spaces. This has been analyzed with the help of the model Lagrangians of Eqs. (34) and (36), following [13]. In these models curvature terms appear that cou-

ple spin and charge fields through cubic terms, *cf.* the last three terms in Eqs. (34) and (36). Again, the form of these Lagrangians maybe understood phenomenologically. In particular, the $SU(2)$ spin-rotational invariance of the models imposes a pairing of the spin fields so that spin and charge fields do not combine in a symmetric way in the cubic terms. When spin and charge parameters are equal ($\gamma_\rho = \gamma_\sigma$) spin simply brings a degeneracy factor of two with respect to the case of spinless fermions. But in the general case, interactions are present in the charge sector ($\gamma_\rho < 1$) while the spin sector is free as there is no backscattering ($\gamma_\sigma = 1$). In this case the spin-charge coupling has non-trivial effects on charge and spin dynamics, *i.e.* charge and spin DSF. The latter were calculated in perturbation theory in curvature, see the corresponding field theories on Figs. 7 and 8. They show a very strong asymmetry of the response of the system with respect to a charge or a spin fluctuation.

The dynamics of the charge degrees of freedom were analyzed with the help of the diagrams of Figs. 9 and 10. These diagrams display the opening of a new channel for the decay of a charge-neutral excitation²³ due to spin-charge coupling. Besides the usual decay into two other charge-neutral excitations, as in the spinless case, a decay into two spin-singlets takes place, see also the corresponding vertex in Fig. 8. The latter lead to a coherent re-arrangement of the background charge around the spin-cone, $\omega = u_\sigma|q|$. As a consequence, our main results, Eq. (39) and the corresponding Fig. 11, show that the charge DSF has a double peak structure: a charge peak at $\omega = u_\rho|q|$ but also a spin peak at $\omega = v|q|$ ²⁶. The charge peak corresponds to an incoherent continuum of single spinless charge-neutral excitations. It has a high-frequency tail corresponding to the incoherent continuum of pairs of these spinless charge-neutral excitations. On the other hand the spin peak corresponds to the incoherent continuum of chargeless single spin-singlet excitations. The latter are free ($\gamma_\sigma = 1$) so the spin peak has no tail. In the limit of strong repulsion, $\gamma_\rho \ll 1$, this spin peak, at $\omega = v|q|$, is therefore well separated from the charge peak at $\omega = u_\rho|q| = v|q|/\gamma_\rho \gg v|q|$.

Similarly, we have analyzed the dynamics of the spin degrees of freedom with the help of the diagrams Figs. 12 and 13. The latter witness the existence of a unique channel of decay of spin (-singlet or triplet) excitations²³: via a pair composed of the spin excitation itself and a charge-neutral excitation, see the corresponding vertex in Fig. 8. The components of this pair travel at different velocities and, as a result, they dissipate spin fluctuations in an incoherent way. This can be seen from our main results, Eqs. (46), (47), (49) and the corresponding Fig. 14. They show that the Tomonaga-Luttinger δ -peak at $\omega = v|q|$ is softened to an algebraic singularity with a transfer of magnetic spectral weight to higher frequencies already at the second order in band-curvature. This continuous transfer extends from the spin frequency $\omega = v|q|$ to the charge frequency $\omega = u_\rho|q|$ with additional tails at $\omega \gg u_\rho|q|$. Because, $u_\rho = v/\gamma_\rho$ is

interaction-dependent the transfer of magnetic spectral weight to higher frequencies increases with increasing interactions, see Fig. 14. At high frequencies, the physical excitations carrying the magnetic spectral weight may be understood as spin-excitations dressed by charge-neutral ones, *cf.* Eq. (51).

At 1/2-filling, the particle-hole symmetry is recovered and the effects resulting from band-curvature, as described above, disappear. In this case higher-order terms in the expansion of Eq. (3) as well as commensurability effects have to be taken into account, *cf.* Ref. [20] in the case of spinless fermions. Moreover, the 1/2-filled case has relations with the physics of quantum spin chains, *e.g.* the large-coupling limit of the 1/2-filled Hubbard model is the anti-ferromagnetic spin chain, and there seemed to be more (non-perturbative) results on correlation functions in this case, *e.g.* Ref. [10]. We leave this case for further studies [27].

Acknowledgments

I thank the Abdus Salam ICTP for hospitality. I am deeply grateful to S. Brazovskii, F. H. L. Essler and A. A. Nersisyan for fruitful discussions.

APPENDIX A: OPERATOR PRODUCT EXPANSIONS

Bosonization rests on the following vertex operator:

$$\psi_\pm(x) = \frac{1}{\sqrt{2\pi}} : \exp \left[\pm i\sqrt{4\pi} \varphi_\pm(x) \right] :,$$

relating the chiral fermionic fields to the chiral bosonic fields. One then needs to express various operators (density, Hamiltonian...) made out of fermions in terms of the bosonic fields. The operators contain the products of fermionic operators at coinciding points and a regularization procedure is required in order to remove the short-distance divergences. This can be achieved by point-splitting the operators, *e.g.*:

$$\psi_\eta^\dagger(x)\psi_\eta(x) = \lim_{\epsilon \rightarrow 0} \left[\psi_\eta^\dagger(x+\epsilon)\psi_\eta(x) - \langle \psi_\eta^\dagger(x+\epsilon)\psi_\eta(x) \rangle \right],$$

where $\eta = \pm$ and:

$$\langle \psi_\pm^\dagger(x+\epsilon)\psi_\pm(x) \rangle = \pm \frac{1}{2\pi i\epsilon}. \quad (\text{A1})$$

The product of vertex operators is normal ordered according to:

$$: e^{i\beta\varphi_\eta(x)} :: e^{i\beta'\varphi_\eta(x')} ::= e^{i\beta\varphi_\eta(x)+i\beta'\varphi_\eta(x')} : e^{-\beta\beta'\langle\varphi_\eta(x)\varphi_\eta(x')\rangle}$$

where:

$$\langle \varphi_\eta(x)\varphi_\eta(x') \rangle = -\frac{1}{4\pi} \ln[i(x-x')]. \quad (\text{A2})$$

Notice that the average values in Eqs. (A1) and (A2) were taken over the TL action, *i.e.* no curvature correction was taken into account. We believe this approximation is sufficient, within the present perturbative approach, to bosonize the theory. Indeed, the first curvature corrections to, *e.g.* Eq. (A2), are in $1/m^2$ while the fermionic Hamiltonian has a contribution in $1/m$. At the level of the current algebra this approximation implies that we keep the usual (ultra-local) commutation relations:

$$[\partial_x \varphi(x), \Pi(x')] = i \partial_x \delta(x - x') + \dots,$$

where the dots correspond to the neglected curvature corrections.

Altogether this yields:

$$\begin{aligned} \rho_\eta(x) &= \psi_\eta^\dagger(x) \psi_\eta(x) \\ &= \text{sgn}(\eta) \lim_{\epsilon \rightarrow 0} \frac{1}{2\pi i \epsilon} \left[e^{-i \text{sgn}(\eta) \sqrt{4\pi} \epsilon \partial_x \varphi_\eta(x)} - 1 \right] \end{aligned}$$

The first OPE reads:

$$\rho_\eta(x) = \psi_\eta^\dagger(x) \psi_\eta(x) = -\frac{1}{\sqrt{\pi}} \partial_x \varphi_\eta(x). \quad (\text{A3})$$

More generally:

$$\begin{aligned} \psi_\eta^\dagger(y) \psi_\eta(x) &= \\ \text{sgn}(\eta) \frac{1}{2\pi i (y-x)} &\left[e^{-i \text{sgn}(\eta) \sqrt{4\pi} [\varphi_\eta(y) - \varphi_\eta(x)]} - 1 \right], \end{aligned}$$

from which:

$$\begin{aligned} \psi_\eta^\dagger(y) \partial_x \psi_\eta(x) &= \\ \text{sgn}(\eta) \frac{1}{2\pi i (y-x)^2} &\left[e^{-i \text{sgn}(\eta) \sqrt{4\pi} [\varphi_\eta(y) - \varphi_\eta(x)]} - 1 \right] \\ + \frac{1}{\sqrt{\pi} (y-x)} &\partial_x \varphi_\eta(x) e^{-i \text{sgn}(\eta) \sqrt{4\pi} [\varphi_\eta(y) - \varphi_\eta(x)]}, \end{aligned}$$

and:

$$\begin{aligned} \psi_\eta^\dagger(y) \partial_{xx} \psi_\eta(x) &= \\ \text{sgn}(\eta) \frac{1}{\pi i (y-x)^3} &\left[e^{-i \text{sgn}(\eta) \sqrt{4\pi} [\varphi_\eta(y) - \varphi_\eta(x)]} - 1 \right] \\ + \frac{2}{\sqrt{\pi} (y-x)^2} &\partial_x \varphi_\eta(x) e^{-i \text{sgn}(\eta) \sqrt{4\pi} [\varphi_\eta(y) - \varphi_\eta(x)]} \\ + \frac{1}{\sqrt{\pi} (y-x)} &\partial_{xx} \varphi_\eta(x) e^{-i \text{sgn}(\eta) \sqrt{4\pi} [\varphi_\eta(y) - \varphi_\eta(x)]} \\ + \text{sgn}(\eta) \frac{2i}{y-x} &(\partial_x \varphi_\eta(x))^2 e^{-i \text{sgn}(\eta) \sqrt{4\pi} [\varphi_\eta(y) - \varphi_\eta(x)]}. \end{aligned}$$

The short-distance products are obtained by setting: $y = x + \epsilon$ and expanding to the lowest meaningful order in ϵ . The diverging terms in $1/\epsilon$ cancel out and as a result the second OPE reads:

$$\psi_\eta^\dagger(x) \partial_x \psi_\eta(x) = -i \text{sgn}(\eta) : (\partial_x \varphi_\eta(x))^2 : - \frac{1}{2\sqrt{\pi}} \partial_{xx} \varphi_\eta(x). \quad (\text{A4})$$

It may be introduced into the Dirac Hamiltonian density:

$$\begin{aligned} \mathcal{H}_{Dirac} &= iv \left[\psi_+^\dagger(x) \partial_x \psi_+(x) - \psi_-^\dagger(x) \partial_x \psi_-(x) \right] \\ &= v \left[: (\partial_x \varphi_+(x))^2 : + : (\partial_x \varphi_-(x))^2 : \right], \end{aligned}$$

where we have neglected the terms which vanish upon integrating over space.

Similarly, the curvature terms read:

$$\begin{aligned} \psi_\eta^\dagger(x + \epsilon) \partial_{xx} \psi_\eta(x) &= \text{sgn}(\eta) \frac{1}{\pi i \epsilon^3} \\ \left[e^{-i \text{sgn}(\eta) \sqrt{4\pi} [\epsilon \partial_x \varphi_\eta(x) + \epsilon^2/2 \partial_{xx} \varphi_\eta(x) + \epsilon^3/6 \partial_{xxx} \varphi_\eta(x)]} - 1 \right] \\ + \frac{2}{\sqrt{\pi} \epsilon^2} &\partial_x \varphi_\eta(x) e^{-i \text{sgn}(\eta) \sqrt{4\pi} [\epsilon \partial_x \varphi_\eta(x) + \epsilon^2/2 \partial_{xx} \varphi_\eta(x)]} \\ + \frac{1}{\sqrt{\pi} \epsilon} &\partial_{xx} \varphi_\eta(x) e^{-i \text{sgn}(\eta) \sqrt{4\pi} \epsilon \partial_x \varphi_\eta(x)} \\ + \text{sgn}(\eta) \frac{2i}{\epsilon} &(\partial_x \varphi_\eta(x))^2 e^{-i \text{sgn}(\eta) \sqrt{4\pi} \epsilon \partial_x \varphi_\eta(x)} \end{aligned}$$

Expanding in ϵ the diverging terms in $1/\epsilon$ and $1/\epsilon^2$ cancel out and the third OPE reads:

$$\begin{aligned} \psi_\eta^\dagger(x) \partial_{xx} \psi_\eta(x) &= \frac{4\sqrt{\pi}}{3} : (\partial_x \varphi_\eta(x))^3 : \\ - 3i \text{sgn}(\eta) &: \partial_x \varphi_\eta(x) \partial_{xx} \varphi_\eta(x) : - \frac{1}{3\sqrt{\pi}} \partial_{xxx} \varphi_\eta(x). \end{aligned} \quad (\text{A5})$$

It may be introduced into the curvature part of the Hamiltonian density:

$$\begin{aligned} \mathcal{H}_{Curvature} &= -\frac{1}{2m} \left[\psi_+^\dagger(x) \partial_{xx} \psi_+(x) + \psi_-^\dagger(x) \partial_{xx} \psi_-(x) \right] \\ &= -\frac{2\sqrt{\pi}}{3m} \left[: (\partial_x \varphi_+(x))^3 : + : (\partial_x \varphi_-(x))^3 : \right], \end{aligned}$$

where we have neglected the terms which vanish upon integrating over space or by symmetry considerations [φ is an odd function of x so that $(\partial_x \varphi)^3$ is even but $\partial_x \varphi \partial_{xx} \varphi$ is odd and does not contribute to the energy].

APPENDIX B: NOTATIONS

Our notations are different from the ones often found in the literature, *cf.* [4,14,20]. They have:

$$\mathcal{H}_{Curvature} = \frac{1}{12\pi m} \left[: (\partial_x \varphi_R(x))^3 : - : (\partial_x \varphi_L(x))^3 : \right],$$

with: $\psi_{R(L)}(x) \sim e^{\pm i k_F x - i \varphi_{R(L)}}$. We have therefore the following correspondence between these notations and our notations:

$$\varphi_+ \rightarrow -\varphi_R / \sqrt{4\pi}, \quad \varphi_- \rightarrow \varphi_L / \sqrt{4\pi}. \quad (\text{B1})$$

We may check that, indeed, this yields the same numerical factor: $(2\sqrt{\pi}/3m)(1/8\pi\sqrt{\pi}) = 1/12\pi m$.

Moreover, the chiral basis, φ_{\pm} , is often used. We which to relate the general irrelevant operator expressed in the φ basis:

$$\partial_x \varphi [n(\partial_\tau \varphi)^2 - v^2(\partial_x \varphi)^2],$$

with its expression in the chiral basis ($n = 3/\gamma_\rho^2$ in the text). In real time this can be done with the help of: $(1/v)\partial_t \varphi = \Pi_\varphi = -\partial_x \varphi_+ + \partial_x \varphi_-$ and $\partial_x \varphi = \partial_x \varphi_+ + \partial_x \varphi_-$, and yields:

$$\begin{aligned} \partial_x \varphi [n(\partial_\tau \varphi)^2 - v^2(\partial_x \varphi)^2] = & \\ -(n+1) [(\partial_x \varphi_+)^2 + (\partial_x \varphi_-)^2] + & \\ +(n-3) [(\partial_x \varphi_+)^2 \partial_x \varphi_- + \partial_x \varphi_+ (\partial_x \varphi_-)^2]. & \end{aligned}$$

The case $n = 3$ corresponds to free fermions:

$$\begin{aligned} \partial_x \varphi [3(\partial_\tau \varphi)^2 - v^2(\partial_x \varphi)^2] &= -4 [(\partial_x \varphi_+)^2 + (\partial_x \varphi_-)^2] \\ &= -\frac{1}{\pi} [(\partial_x \varphi_R)^2 + (\partial_x \varphi_L)^2], \quad \text{where Eq. (B1) has been used.} \end{aligned}$$

and is the sum of two chiral terms. This implies that tails are in the crossed chiral terms. They can be isolated by a special (unrealistic) choice of the interactions: $n = -1$, which yields:

$$\begin{aligned} \partial_x \varphi [(\partial_\tau \varphi)^2 + v^2(\partial_x \varphi)^2] = & \\ 4 [(\partial_x \varphi_+)^2 \partial_x \varphi_- + \partial_x \varphi_+ (\partial_x \varphi_-)^2] = & \\ \frac{1}{\pi\sqrt{4\pi}} [(\partial_x \varphi_R)^2 \partial_x \varphi_L - \partial_x \varphi_R (\partial_x \varphi_L)^2], & \end{aligned}$$

APPENDIX C: CORRELATION FUNCTIONS IN THE SPINLESS FERMION CASE

1. Second-order perturbation in curvature: φ -representation

The second order correlation function reads:

$$\begin{aligned} \langle |\varphi(i\omega, q)|^2 \rangle^{(2)} &= \frac{1}{2(m'u_\rho^2)^2} \frac{1}{\beta^6} \sum_{\omega_1, \omega_2, \omega_3, \omega'_1, \omega'_2, \omega'_3} \int \frac{dq_1 dq_2 dq_3}{(2\pi)^3} \frac{dq'_1 dq'_2 dq'_3}{(2\pi)^3} \delta[1+2+3] \delta[1'+2'+3'] \\ & [n_\rho q_1 \omega_2 \omega_3 - u_\rho^2 q_1 q_2 q_3] [n_\rho q'_1 \omega'_2 \omega'_3 - u_\rho^2 q'_1 q'_2 q'_3] \langle \varphi_\omega(q) \varphi_{-\omega}(-q) \varphi_{\omega_1}(q_1) \varphi_{\omega_2}(q_2) \varphi_{\omega_3}(q_3) \varphi_{\omega'_1}(q'_1) \varphi_{\omega'_2}(q'_2) \varphi_{\omega'_3}(q'_3) \rangle_0, \end{aligned}$$

where $n_\rho = 3/\gamma_\rho^2$ and may be conveniently split into three contributions:

$$\begin{aligned} \langle |\varphi(i\omega, q)|^2 \rangle_A^{(2)} &= \frac{u_\rho^4}{2(m'u_\rho^2)^2} \frac{1}{\beta^6} \sum_{\omega_1, \omega_2, \omega_3, \omega'_1, \omega'_2, \omega'_3} \int \frac{dq_1 dq_2 dq_3}{(2\pi)^3} \frac{dq'_1 dq'_2 dq'_3}{(2\pi)^3} \delta[1+2+3] \delta[1'+2'+3'] \\ & q_1 q_2 q_3 q'_1 q'_2 q'_3 \langle \varphi_\omega(q) \varphi_{-\omega}(-q) \varphi_{\omega_1}(q_1) \varphi_{\omega_2}(q_2) \varphi_{\omega_3}(q_3) \varphi_{\omega'_1}(q'_1) \varphi_{\omega'_2}(q'_2) \varphi_{\omega'_3}(q'_3) \rangle_0, \end{aligned}$$

$$\begin{aligned} \langle |\varphi(i\omega, q)|^2 \rangle_B^{(2)} &= \frac{n_\rho^2}{2(m'u_\rho^2)^2} \frac{1}{\beta^6} \sum_{\omega_1, \omega_2, \omega_3, \omega'_1, \omega'_2, \omega'_3} \int \frac{dq_1 dq_2 dq_3}{(2\pi)^3} \frac{dq'_1 dq'_2 dq'_3}{(2\pi)^3} \delta[1+2+3] \delta[1'+2'+3'] \\ & q_1 \omega_2 \omega_3 q'_1 \omega'_2 \omega'_3 \langle \varphi_\omega(q) \varphi_{-\omega}(-q) \varphi_{\omega_1}(q_1) \varphi_{\omega_2}(q_2) \varphi_{\omega_3}(q_3) \varphi_{\omega'_1}(q'_1) \varphi_{\omega'_2}(q'_2) \varphi_{\omega'_3}(q'_3) \rangle_0, \end{aligned}$$

$$\begin{aligned} \langle |\varphi(i\omega, q)|^2 \rangle_C^{(2)} &= -\frac{n_\rho u_\rho^2}{(m'u_\rho^2)^2} \frac{1}{\beta^6} \sum_{\omega_1, \omega_2, \omega_3, \omega'_1, \omega'_2, \omega'_3} \int \frac{dq_1 dq_2 dq_3}{(2\pi)^3} \frac{dq'_1 dq'_2 dq'_3}{(2\pi)^3} \delta[1+2+3] \delta[1'+2'+3'] \\ & q_1 \omega_2 \omega_3 q'_1 q'_2 q'_3 \langle \varphi_\omega(q) \varphi_{-\omega}(-q) \varphi_{\omega_1}(q_1) \varphi_{\omega_2}(q_2) \varphi_{\omega_3}(q_3) \varphi_{\omega'_1}(q'_1) \varphi_{\omega'_2}(q'_2) \varphi_{\omega'_3}(q'_3) \rangle_0. \end{aligned}$$

The first contribution is easy to Wick order and yields:

$$\langle |\varphi(i\omega, q)|^2 \rangle_A^{(2)} = \frac{18q^2 u_\rho^4}{(m'u_\rho^2)^2} [\mathcal{D}(i\omega, q)]^2 \frac{1}{\beta} \sum_\nu \int \frac{dp}{2\pi} p^2 (p-q)^2 \mathcal{D}(i\nu, p) \mathcal{D}(i\nu - i\omega, p-q).$$

The imaginary part of the corresponding retarded self-energy reads:

$$\begin{aligned}\Im\Sigma_A^R(\omega, q) &= \frac{3}{8u_\rho} \left(\frac{v}{u_\rho}\right)^2 \left(\frac{q^2}{m'}\right)^2 u_\rho q [\delta[\omega - u_\rho q] - \delta[\omega + u_\rho q]] \\ &+ \frac{9}{16u_\rho} \left(\frac{v}{u_\rho}\right)^2 \left(\frac{q}{m'u_\rho}\right)^2 [\omega^2 - (u_\rho q)^2] \mathcal{F}_\rho(\omega, q),\end{aligned}\quad (\text{C1})$$

where \mathcal{F}_ρ is given by Eq. (28). The second correlation function is simplified as:

$$\begin{aligned}\langle |\varphi(i\omega, q)|^2 \rangle_B^{(2)} &= \frac{2n_\rho^2 q^2}{(m'u_\rho^2)^2} [\mathcal{D}(i\omega, q)]^2 \frac{1}{\beta} \sum_\nu \int \frac{dp}{2\pi} \nu^2 (\nu - \omega)^2 \mathcal{D}(i\nu, p) \mathcal{D}(i\nu - i\omega, p - q) \\ &+ \frac{8n_\rho^2 q\omega}{(m'u_\rho^2)^2} [\mathcal{D}(i\omega, q)]^2 \frac{1}{\beta} \sum_\nu \int \frac{dp}{2\pi} p\nu (\nu - \omega)^2 \mathcal{D}(i\nu, p) \mathcal{D}(i\nu - i\omega, p - q) \\ &+ \frac{4n_\rho^2 \omega^2}{(m'u_\rho^2)^2} [\mathcal{D}(i\omega, q)]^2 \frac{1}{\beta} \sum_\nu \int \frac{dp}{2\pi} p^2 (\nu - \omega)^2 \mathcal{D}(i\nu, p) \mathcal{D}(i\nu - i\omega, p - q) \\ &+ \frac{4n_\rho^2 \omega^2}{(m'u_\rho^2)^2} [\mathcal{D}(i\omega, q)]^2 \frac{1}{\beta} \sum_\nu \int \frac{dp}{2\pi} p(p - q)\nu (\nu - \omega) \mathcal{D}(i\nu, p) \mathcal{D}(i\nu - i\omega, p - q).\end{aligned}$$

All terms contribute to the on-shell part of the correlation function but only the first contributes to the off-shell part. The result for the self-energy part reads:

$$\begin{aligned}\Im\Sigma_B^R(\omega, q) &= \frac{3n_\rho^2}{8u_\rho} \left(\frac{v}{u_\rho}\right)^2 \left(\frac{q^2}{m'}\right)^2 u_\rho q [\delta[\omega - u_\rho q] - \delta[\omega + u_\rho q]] \\ &+ \frac{n_\rho^2}{16u_\rho} \left(\frac{v}{u_\rho}\right)^2 \left(\frac{q}{m'u_\rho}\right)^2 [\omega^2 - (u_\rho q)^2] \mathcal{F}_\rho(\omega, q).\end{aligned}\quad (\text{C2})$$

Finally, the third correlation function is simplified as:

$$\begin{aligned}\langle |\varphi(i\omega, q)|^2 \rangle_C^{(2)} &= -\frac{12n_\rho u_\rho^2 q^2}{(m'u_\rho^2)^2} [\mathcal{D}(i\omega, q)]^2 \frac{1}{\beta} \sum_\nu \int \frac{dp}{2\pi} p(p - q)\nu (\nu - \omega) \mathcal{D}(i\nu, p) \mathcal{D}(i\nu - i\omega, p - q) \\ &- \frac{24n_\rho u_\rho^2 q\omega}{(m'u_\rho^2)^2} [\mathcal{D}(i\omega, q)]^2 \frac{1}{\beta} \sum_\nu \int \frac{dp}{2\pi} p^2 (p - q)(\nu - \omega) \mathcal{D}(i\nu, p) \mathcal{D}(i\nu - i\omega, p - q).\end{aligned}$$

Again, only the first term (which carries the q^2 factor) contributes to the off-shell part whereas both contribute to the on-shell part. The corresponding self-energy part reads:

$$\begin{aligned}\Im\Sigma_C^R(\omega, q) &= \frac{3n_\rho}{4u_\rho} \left(\frac{v}{u_\rho}\right)^2 \left(\frac{q^2}{m'}\right)^2 u_\rho q [\delta[\omega - u_\rho q] - \delta[\omega + u_\rho q]] \\ &- \frac{3n_\rho}{8u_\rho} \left(\frac{v}{u_\rho}\right)^2 \left(\frac{q}{m'u_\rho}\right)^2 [\omega^2 - (u_\rho q)^2] \mathcal{F}_\rho(\omega, q).\end{aligned}\quad (\text{C3})$$

Adding the above self-energy parts the factors $(1 + n_\rho)^2 = (1 + 3/\gamma_\rho^2)^2$ and $(3 - n_\rho)^2 = 9(1 - 1/\gamma_\rho^2)^2$ appear and the self-energy is given by Eq. (27).

2. Second-order perturbation in curvature: φ, θ -representation

Expanding the perturbation up to second order yields three contributions:

$$\begin{aligned}
\langle |\varphi(i\omega, q)|^2 \rangle^{(2)} &= \frac{1}{2m'^2} \frac{1}{\beta^6} \sum_{\omega_1, \omega_2, \omega_3, \omega'_1, \omega'_2, \omega'_3} \int \frac{dq_1 dq_2 dq_3}{(2\pi)^3} \frac{dq'_1 dq'_2 dq'_3}{(2\pi)^3} \delta[1+2+3] \delta[1'+2'+3'] \\
& q_1 q_2 q_3 q'_1 q'_2 q'_3 \langle \varphi_\omega(q) \varphi_{-\omega}(-q) \varphi_{\omega_1}(q_1) \varphi_{\omega_2}(q_2) \varphi_{\omega_3}(q_3) \varphi_{\omega'_1}(q'_1) \varphi_{\omega'_2}(q'_2) \varphi_{\omega'_3}(q'_3) \rangle_0, \\
& + \frac{9}{2m'^2} \frac{1}{\beta^6} \sum_{\omega_1, \omega_2, \omega_3, \omega'_1, \omega'_2, \omega'_3} \int \frac{dq_1 dq_2 dq_3}{(2\pi)^3} \frac{dq'_1 dq'_2 dq'_3}{(2\pi)^3} \delta[1+2+3] \delta[1'+2'+3'] \\
& q_1 q_2 q_3 q'_1 q'_2 q'_3 \langle \varphi_\omega(q) \varphi_{-\omega}(-q) \varphi_{\omega_1}(q_1) \theta_{\omega_2}(q_2) \theta_{\omega_3}(q_3) \varphi_{\omega'_1}(q'_1) \theta_{\omega'_2}(q'_2) \theta_{\omega'_3}(q'_3) \rangle_0, \\
& + \frac{3}{m'^2} \frac{1}{\beta^6} \sum_{\omega_1, \omega_2, \omega_3, \omega'_1, \omega'_2, \omega'_3} \int \frac{dq_1 dq_2 dq_3}{(2\pi)^3} \frac{dq'_1 dq'_2 dq'_3}{(2\pi)^3} \delta[1+2+3] \delta[1'+2'+3'] \\
& q_1 q_2 q_3 q'_1 q'_2 q'_3 \langle \varphi_\omega(q) \varphi_{-\omega}(-q) \varphi_{\omega_1}(q_1) \theta_{\omega_2}(q_2) \theta_{\omega_3}(q_3) \varphi_{\omega'_1}(q'_1) \varphi_{\omega'_2}(q'_2) \varphi_{\omega'_3}(q'_3) \rangle_0.
\end{aligned}$$

The first contribution is exactly the same as the A -term of the previous paragraph.

Wick ordering the next contributions we classify the diagrams according to the number of θ -wings, see Fig. 5. Diagrams with no θ -wing are labeled as SLA (SpinLess A). SLA1 corresponds to the previous A term. The next terms read:

$$\begin{aligned}
\mathcal{D}_{A2\varphi\varphi}^{(2)}(i\omega, q) &= -18 [\mathcal{D}_{\varphi\varphi}^{(0)}(i\omega, q)]^2 \left(\frac{q}{m'}\right)^2 \frac{1}{\beta} \sum_{\nu} \int \frac{dp}{2\pi} p^2 (p-q)^2 \mathcal{D}_{\theta\theta}^{(0)}(i\nu, p) \mathcal{D}_{\theta\theta}^{(0)}(i\nu - i\omega, p - q) \\
\mathcal{D}_{A3\varphi\varphi}^{(2)}(i\omega, q) &= -36 [\mathcal{D}_{\varphi\varphi}^{(0)}(i\omega, q)]^2 \left(\frac{q}{m'}\right)^2 \frac{1}{\beta} \sum_{\nu} \int \frac{dp}{2\pi} p^2 (p-q)^2 \mathcal{D}_{\varphi\theta}^{(0)}(i\nu, p) \mathcal{D}_{\theta\varphi}^{(0)}(i\nu - i\omega, p - q).
\end{aligned}$$

Their self-energy parts reads:

$$\begin{aligned}
\Im \Sigma_{A1}^R(\omega, q) &= \frac{3\gamma_\rho^2}{8u_\rho} \left(\frac{q^2}{m'}\right)^2 u_\rho q [\delta[\omega - u_\rho q] - \delta[\omega + u_\rho q]] \\
&+ \frac{9\gamma_\rho^2}{16u_\rho} \left(\frac{q}{m'u_\rho}\right)^2 [\omega^2 - (u_\rho q)^2] \mathcal{F}_\rho(\omega, q), \\
\Im \Sigma_{A2}^R(\omega, q) &= \frac{3}{8u_\rho \gamma_\rho^2} \left(\frac{q^2}{m'}\right)^2 u_\rho q [\delta[\omega - u_\rho q] - \delta[\omega + u_\rho q]] \\
&+ \frac{9}{16u_\rho \gamma_\rho^2} \left(\frac{q}{m'u_\rho}\right)^2 [\omega^2 - (u_\rho q)^2] \mathcal{F}_\rho(\omega, q), \\
\Im \Sigma_{A3}^R(\omega, q) &= \frac{3}{4u_\rho} \left(\frac{q^2}{m'}\right)^2 u_\rho q [\delta[\omega - u_\rho q] - \delta[\omega + u_\rho q]] \\
&- \frac{9}{8u_\rho} \left(\frac{q}{m'u_\rho}\right)^2 [\omega^2 - (u_\rho q)^2] \mathcal{F}_\rho(\omega, q).
\end{aligned}$$

Diagrams with one θ -wing (SLB) read:

$$\begin{aligned}
\mathcal{D}_{B1\varphi\varphi}^{(2)}(i\omega, q) &= 72 \mathcal{D}_{\varphi\theta}^{(0)}(i\omega, q) \mathcal{D}_{\varphi\varphi}^{(0)}(i\omega, q) \left(\frac{q}{m'}\right)^2 \frac{1}{\beta} \sum_{\nu} \int \frac{dp}{2\pi} p^2 (p-q)^2 \mathcal{D}_{\varphi\theta}^{(0)}(i\nu, p) \mathcal{D}_{\theta\theta}^{(0)}(i\nu - i\omega, p - q) \\
\mathcal{D}_{B2\varphi\varphi}^{(2)}(i\omega, q) &= -72 \mathcal{D}_{\varphi\theta}^{(0)}(i\omega, q) \mathcal{D}_{\varphi\varphi}^{(0)}(i\omega, q) \left(\frac{q}{m'}\right)^2 \frac{1}{\beta} \sum_{\nu} \int \frac{dp}{2\pi} p^2 (p-q)^2 \mathcal{D}_{\varphi\theta}^{(0)}(i\nu, p) \mathcal{D}_{\varphi\varphi}^{(0)}(i\nu - i\omega, p - q).
\end{aligned}$$

The corresponding self-energy parts read:

$$\begin{aligned}
\Im \Sigma_{B1}^R(\omega, q) &= \frac{3}{2u_\rho \gamma_\rho^2} \left(\frac{q^2}{m'}\right)^2 u_\rho q [\delta[\omega - u_\rho q] - \delta[\omega + u_\rho q]], \\
\Im \Sigma_{B2}^R(\omega, q) &= \frac{3}{2u_\rho} \left(\frac{q^2}{m'}\right)^2 u_\rho q [\delta[\omega - u_\rho q] - \delta[\omega + u_\rho q]].
\end{aligned}$$

Diagrams with two θ -wings (SLC) read:

$$\begin{aligned} \mathcal{D}_{C1\varphi\varphi}^{(2)}(i\omega, q) &= 36 [\mathcal{D}_{\varphi\theta}^{(0)}(i\omega, q)]^2 \left(\frac{q}{m'}\right)^2 \frac{1}{\beta} \sum_{\nu} \int \frac{dp}{2\pi} p^2(p-q)^2 \mathcal{D}_{\varphi\varphi}^{(0)}(i\nu, p) \mathcal{D}_{\theta\theta}^{(0)}(i\nu - i\omega, p - q) \\ &+ 36 [\mathcal{D}_{\varphi\theta}^{(0)}(i\omega, q)]^2 \left(\frac{q}{m'}\right)^2 \frac{1}{\beta} \sum_{\nu} \int \frac{dp}{2\pi} p^2(p-q)^2 \mathcal{D}_{\varphi\theta}^{(0)}(i\nu, p) \mathcal{D}_{\varphi\theta}^{(0)}(i\nu - i\omega, p - q). \end{aligned}$$

The corresponding self-energy parts read:

$$\begin{aligned} \Im\Sigma_{C1}^R(\omega, q) &= \frac{3}{4u_{\rho}\gamma_{\rho}^2} \left(\frac{q^2}{m'}\right)^2 u_{\rho}q [\delta[\omega - u_{\rho}q] - \delta[\omega + u_{\rho}q]] \\ &+ \frac{9}{8u_{\rho}\gamma_{\rho}^2} \left(\frac{q}{m'u_{\rho}}\right)^2 [\omega^2 - (u_{\rho}q)^2] \mathcal{F}_{\rho}(\omega, q), \\ \Im\Sigma_{C2}^R(\omega, q) &= \frac{3}{4u_{\rho}\gamma_{\rho}^2} \left(\frac{q^2}{m'}\right)^2 u_{\rho}q [\delta[\omega - u_{\rho}q] - \delta[\omega + u_{\rho}q]] \\ &- \frac{9}{8u_{\rho}\gamma_{\rho}^2} \left(\frac{q}{m'u_{\rho}}\right)^2 [\omega^2 - (u_{\rho}q)^2] \mathcal{F}_{\rho}(\omega, q). \end{aligned}$$

The total contribution of each set read:

$$\begin{aligned} \Im\Sigma_A^R(\omega, q) &= \frac{3\gamma_{\rho}^2}{8u_{\rho}} \left[1 + \frac{1}{\gamma_{\rho}^2}\right]^2 \left(\frac{q^2}{m'}\right)^2 u_{\rho}q [\delta[\omega - u_{\rho}q] - \delta[\omega + u_{\rho}q]] \\ &+ \frac{9\gamma_{\rho}^2}{16u_{\rho}} \left[1 - \frac{1}{\gamma_{\rho}^2}\right]^2 \left(\frac{q}{m'u_{\rho}}\right)^2 [\omega^2 - (u_{\rho}q)^2] \mathcal{F}_{\rho}(\omega, q) \\ \Im\Sigma_B^R(\omega, q) &= \frac{3}{2u_{\rho}} \left[1 + \frac{1}{\gamma_{\rho}^2}\right] \left(\frac{q^2}{m'}\right)^2 u_{\rho}q [\delta[\omega - u_{\rho}q] - \delta[\omega + u_{\rho}q]] \\ \Im\Sigma_C^R(\omega, q) &= \frac{3}{2u_{\rho}\gamma_{\rho}^2} \left(\frac{q^2}{m'}\right)^2 u_{\rho}q [\delta[\omega - u_{\rho}q] - \delta[\omega + u_{\rho}q]]. \end{aligned} \quad (C4)$$

It is interesting to see that all diagrams contribute to the on-shell self-energy; however, the final expression for the tail comes only from the SLA set, *i.e.* those diagrams with no θ -wings. The set SLB with a single θ -wing does not have any off-shell contribution whereas the set SLC with two θ -wings has off-shell contributions which cancel each-other. Notice that if the latter had a net contribution to the tails, this contribution would have higher powers of frequency which would violate the f-sum rule. In dimensionless units these additional contributions are: $\propto \omega/u_{\rho}q$ for SLB and $\propto (\omega/u_{\rho}q)^2$ for SLC due to the presence of a single θ -wing and two θ -wings. On-shell, *i.e.* for $\omega = \pm u_{\rho}q$, such contributions are ± 1 which yield the correct signs in front of the delta functions.

Adding all the above self-energies yields:

$$\begin{aligned} \Im\Sigma_{\rho}^R(\omega, q) &= \frac{3\gamma_{\rho}^2}{8u_{\rho}} \left[1 + \frac{3}{\gamma_{\rho}^2}\right]^2 \left(\frac{q^2}{m'}\right)^2 u_{\rho}q [\delta[\omega - u_{\rho}q] - \delta[\omega + u_{\rho}q]] \\ &+ \frac{9\gamma_{\rho}^2}{16u_{\rho}} \left[1 - \frac{1}{\gamma_{\rho}^2}\right]^2 \left(\frac{q}{m'u_{\rho}}\right)^2 [\omega^2 - (u_{\rho}q)^2] \mathcal{F}_{\rho}(\omega, q). \end{aligned} \quad (C5)$$

Substituting $m' = 6m/\sqrt{\pi}$ yields Eq. (27) which is precisely what has been found in the previous paragraph.

APPENDIX D: CORRELATION FUNCTIONS IN THE SPINFUL FERMION CASE

1. Charge structure factor

With the help of the Lagrangian Eq. (34) the second-order contributions to the charge phase correlator have three contributions:

$$\langle |\varphi(i\omega, q)|^2 \rangle_A^{(2)} = \text{Similar to the spinless case,}$$

which is identical to what is found in the spinless case,

$$\begin{aligned}
& \langle |\varphi(i\omega, q)|^2 \rangle_B^{(2)} = \\
& -18 [\mathcal{D}_{\varphi\varphi}^{(0)}(i\omega, q)]^2 \left(\frac{q}{m'}\right)^2 \frac{1}{\beta} \sum_{\nu} \int \frac{dp}{2\pi} p^2(p-q)^2 \mathcal{D}_{\sigma\sigma}^{(0)}(i\nu, p) \mathcal{D}_{\sigma\sigma}^{(0)}(i\nu - i\omega, p-q) \\
& -36 [\mathcal{D}_{\varphi\varphi}^{(0)}(i\omega, q)]^2 \left(\frac{q}{m'}\right)^2 \frac{1}{\beta} \sum_{\nu} \int \frac{dp}{2\pi} p^2(p-q)^2 \mathcal{D}_{\sigma\theta\sigma}^{(0)}(i\nu, p) \mathcal{D}_{\sigma\theta\sigma}^{(0)}(i\nu - i\omega, p-q) \\
& -18 [\mathcal{D}_{\varphi\varphi}^{(0)}(i\omega, q)]^2 \left(\frac{q}{m'}\right)^2 \frac{1}{\beta} \sum_{\nu} \int \frac{dp}{2\pi} p^2(p-q)^2 \mathcal{D}_{\theta\sigma\theta\sigma}^{(0)}(i\nu, p) \mathcal{D}_{\theta\sigma\theta\sigma}^{(0)}(i\nu - i\omega, p-q),
\end{aligned}$$

$$\begin{aligned}
& \langle |\varphi(i\omega, q)|^2 \rangle_C^{(2)} = \\
& -72 \mathcal{D}_{\varphi\varphi}^{(0)}(i\omega, q) \mathcal{D}_{\varphi\theta\rho}^{(0)}(i\omega, q) \left(\frac{q}{m'}\right)^2 \frac{1}{\beta} \sum_{\nu} \int \frac{dp}{2\pi} p^2(p-q)^2 \mathcal{D}_{\theta\sigma\sigma}^{(0)}(i\nu, p) \mathcal{D}_{\theta\sigma\theta\sigma}^{(0)}(i\nu - i\omega, p-q) \\
& -72 \mathcal{D}_{\varphi\varphi}^{(0)}(i\omega, q) \mathcal{D}_{\varphi\theta\rho}^{(0)}(i\omega, q) \left(\frac{q}{m'}\right)^2 \frac{1}{\beta} \sum_{\nu} \int \frac{dp}{2\pi} p^2(p-q)^2 \mathcal{D}_{\sigma\sigma}^{(0)}(i\nu, p) \mathcal{D}_{\sigma\theta\sigma}^{(0)}(i\nu - i\omega, p-q)
\end{aligned}$$

$$\begin{aligned}
& \langle |\varphi(i\omega, q)|^2 \rangle_D^{(2)} = \\
& -36 [\mathcal{D}_{\varphi\theta\rho}^{(0)}(i\omega, q)]^2 \left(\frac{q}{m'}\right)^2 \frac{1}{\beta} \sum_{\nu} \int \frac{dp}{2\pi} p^2(p-q)^2 \mathcal{D}_{\sigma\sigma}^{(0)}(i\nu, p) \mathcal{D}_{\theta\sigma\theta\sigma}^{(0)}(i\nu - i\omega, p-q) \\
& -36 [\mathcal{D}_{\varphi\theta\rho}^{(0)}(i\omega, q)]^2 \left(\frac{q}{m'}\right)^2 \frac{1}{\beta} \sum_{\nu} \int \frac{dp}{2\pi} p^2(p-q)^2 \mathcal{D}_{\sigma\theta\sigma}^{(0)}(i\nu, p) \mathcal{D}_{\theta\sigma\sigma}^{(0)}(i\nu - i\omega, p-q).
\end{aligned}$$

Based on the similarity of the calculation with the spinless case we directly give the expression of the various self-energy parts:

$$\begin{aligned}
\Im\Sigma_B^R(\omega, q) &= \frac{3\gamma_\sigma^2}{8u_\sigma} \left(1 + \frac{1}{\gamma_\sigma^2}\right)^2 \left(\frac{q^2}{m'}\right)^2 u_\sigma q [\delta[\omega - u_\sigma q] - \delta[\omega + u_\sigma q]] \\
&+ \frac{9\gamma_\sigma^2}{16u_\sigma} \left(1 - \frac{1}{\gamma_\sigma^2}\right)^2 \left(\frac{q}{m'u_\sigma}\right)^2 [\omega^2 - (u_\sigma q)^2] \mathcal{F}_\sigma(\omega, q). \\
\Im\Sigma_C^R(\omega, q) &= \frac{3\gamma_\sigma}{2u_\sigma\gamma_\rho} \left[1 + \frac{1}{\gamma_\sigma^2}\right] \left(\frac{q^2}{m'}\right)^2 u_\sigma q [\delta[\omega - u_\sigma q] - \delta[\omega + u_\sigma q]] \\
\Im\Sigma_D^R(\omega, q) &= \frac{3}{2u_\sigma\gamma_\rho^2} \left(\frac{q^2}{m'}\right)^2 u_\sigma q [\delta[\omega - u_\sigma q] - \delta[\omega + u_\sigma q]], \tag{D1}
\end{aligned}$$

where \mathcal{F}_σ is given by Eq. (38). Notice that these expressions satisfy the basic properties of the diagrams with zero, one or two θ -wings.

Adding all the above self-energies and substituting $m' = 6m/\sqrt{\pi}$ yields:

$$\begin{aligned}
\Im\Sigma_\rho^R(\omega, q) &= \frac{\gamma_\sigma^2\pi}{96u_\sigma} \left[1 + \frac{1}{\gamma_\sigma^2} + \frac{2}{\gamma_\sigma\gamma_\rho}\right]^2 \left(\frac{q^2}{m}\right)^2 u_\sigma q [\delta[\omega - u_\sigma q] - \delta[\omega + u_\sigma q]] \\
&+ \frac{\gamma_\sigma^2\pi}{64u_\sigma} \left[1 - \frac{1}{\gamma_\sigma^2}\right]^2 \left(\frac{q}{mu_\sigma}\right)^2 [\omega^2 - (u_\sigma q)^2] \mathcal{F}_\sigma(\omega, q). \tag{D2}
\end{aligned}$$

Adding the part arising from the charge degrees of freedom, the total self-energy of interacting spinful fermions is given by Eq. (37).

2. Spin structure factor

With the help of the Lagrangian Eq. (34) the second-order contributions to the self-energy part of the spin structure factor read:

$$\begin{aligned} \Sigma_A^{(2)}(i\omega, q) = & \\ & 36 \left(\frac{q}{m'}\right)^2 \frac{1}{\beta} \sum_{\nu} \int \frac{dp}{2\pi} p^2(p-q)^2 \mathcal{D}_{\varphi\varphi}^{(0)}(i\nu, p) \mathcal{D}_{\sigma\sigma}^{(0)}(i\nu - i\omega, p - q) \\ & 36 \left(\frac{q}{m'}\right)^2 \frac{1}{\beta} \sum_{\nu} \int \frac{dp}{2\pi} p^2(p-q)^2 \mathcal{D}_{\theta_\varphi\theta_\varphi}^{(0)}(i\nu, p) \mathcal{D}_{\theta_\sigma\theta_\sigma}^{(0)}(i\nu - i\omega, p - q) \\ & 72 \left(\frac{q}{m'}\right)^2 \frac{1}{\beta} \sum_{\nu} \int \frac{dp}{2\pi} p^2(p-q)^2 \mathcal{D}_{\varphi\theta_\varphi}^{(0)}(i\nu, p) \mathcal{D}_{\sigma\theta_\sigma}^{(0)}(i\nu - i\omega, p - q), \end{aligned}$$

$$\begin{aligned} \Sigma_B^{(2)}(i\omega, q) = & \\ & \frac{72}{\gamma_\sigma} \frac{i\omega}{u_\sigma q} \left(\frac{q}{m'}\right)^2 \frac{1}{\beta} \sum_{\nu} \int \frac{dp}{2\pi} p^2(p-q)^2 \mathcal{D}_{\varphi\varphi}^{(0)}(i\nu, p) \mathcal{D}_{\sigma\theta_\sigma}^{(0)}(i\nu - i\omega, p - q) \\ & \frac{72}{\gamma_\sigma} \frac{i\omega}{u_\sigma q} \left(\frac{q}{m'}\right)^2 \frac{1}{\beta} \sum_{\nu} \int \frac{dp}{2\pi} p^2(p-q)^2 \mathcal{D}_{\theta_\varphi\theta_\varphi}^{(0)}(i\nu, p) \mathcal{D}_{\sigma\theta_\sigma}^{(0)}(i\nu - i\omega, p - q) \\ & \frac{72}{\gamma_\sigma} \frac{i\omega}{u_\sigma q} \left(\frac{q}{m'}\right)^2 \frac{1}{\beta} \sum_{\nu} \int \frac{dp}{2\pi} p^2(p-q)^2 \mathcal{D}_{\varphi\theta_\varphi}^{(0)}(i\nu, p) \mathcal{D}_{\sigma\sigma}^{(0)}(i\nu - i\omega, p - q), \\ & \frac{72}{\gamma_\sigma} \frac{i\omega}{u_\sigma q} \left(\frac{q}{m'}\right)^2 \frac{1}{\beta} \sum_{\nu} \int \frac{dp}{2\pi} p^2(p-q)^2 \mathcal{D}_{\varphi\theta_\varphi}^{(0)}(i\nu, p) \mathcal{D}_{\theta_\sigma\theta_\sigma}^{(0)}(i\nu - i\omega, p - q), \end{aligned}$$

$$\begin{aligned} \Sigma_C^{(2)}(i\omega, q) = & \\ & \frac{36}{\gamma_\sigma^2} \left(\frac{i\omega}{u_\sigma q}\right)^2 \left(\frac{q}{m'}\right)^2 \frac{1}{\beta} \sum_{\nu} \int \frac{dp}{2\pi} p^2(p-q)^2 \mathcal{D}_{\varphi\varphi}^{(0)}(i\nu, p) \mathcal{D}_{\theta_\sigma\theta_\sigma}^{(0)}(i\nu - i\omega, p - q) \\ & \frac{36}{\gamma_\sigma^2} \left(\frac{i\omega}{u_\sigma q}\right)^2 \left(\frac{q}{m'}\right)^2 \frac{1}{\beta} \sum_{\nu} \int \frac{dp}{2\pi} p^2(p-q)^2 \mathcal{D}_{\theta_\varphi\theta_\varphi}^{(0)}(i\nu, p) \mathcal{D}_{\sigma\sigma}^{(0)}(i\nu - i\omega, p - q) \\ & \frac{72}{\gamma_\sigma^2} \left(\frac{i\omega}{u_\sigma q}\right)^2 \left(\frac{q}{m'}\right)^2 \frac{1}{\beta} \sum_{\nu} \int \frac{dp}{2\pi} p^2(p-q)^2 \mathcal{D}_{\varphi\theta_\varphi}^{(0)}(i\nu, p) \mathcal{D}_{\sigma\theta_\sigma}^{(0)}(i\nu - i\omega, p - q). \end{aligned}$$

The corresponding imaginary parts read:

$$\begin{aligned} \Im\Sigma_A^R(\omega, q) = & \frac{9}{2u_\sigma} \gamma_\rho\gamma_\sigma \left[1 + \frac{1}{\gamma_\rho\gamma_\sigma}\right]^2 \left(\frac{q^2}{m'}\right)^2 u_\sigma q \frac{1}{|u_\rho - u_\sigma|^3 q^3} \\ & \left\{ [\omega - u_\sigma q] [\omega - u_\rho q] \left[n_B \left[\frac{u_\rho[\omega - u_\sigma q]}{u_\rho - u_\sigma} \right] - n_B \left[\frac{u_\sigma[\omega - u_\rho q]}{u_\rho - u_\sigma} \right] \right] \right. \\ & \left. + [\omega + u_\sigma q] [\omega + u_\rho q] \left[n_B \left[\frac{u_\rho[\omega + u_\sigma q]}{u_\rho - u_\sigma} \right] - n_B \left[\frac{u_\sigma[\omega + u_\rho q]}{u_\rho - u_\sigma} \right] \right] \right\} \\ & + \frac{9}{2} \gamma_\rho\gamma_\sigma \left[1 - \frac{1}{\gamma_\rho\gamma_\sigma}\right]^2 \left(\frac{q}{m'}\right)^2 \frac{1}{|u_\rho + u_\sigma|^3 q^3} \\ & \left\{ [\omega + u_\sigma q] [\omega - u_\rho q] \left[n_B \left[-\frac{u_\sigma[\omega - u_\rho q]}{u_\rho + u_\sigma} \right] - n_B \left[\frac{u_\rho[\omega + u_\sigma q]}{u_\rho + u_\sigma} \right] \right] \right. \\ & \left. + [\omega - u_\sigma q] [\omega + u_\rho q] \left[n_B \left[-\frac{u_\sigma[\omega + u_\rho q]}{u_\rho + u_\sigma} \right] - n_B \left[\frac{u_\rho[\omega - u_\sigma q]}{u_\rho + u_\sigma} \right] \right] \right\}, \end{aligned} \tag{D3}$$

$$\begin{aligned}
\Im\Sigma_B^R(\omega, q) &= \frac{9}{u_\sigma\gamma_\sigma} \left[\gamma_\rho + \gamma_\sigma + \frac{1}{\gamma_\rho} + \frac{1}{\gamma_\sigma} \right] \frac{\omega}{u_\sigma q} \left(\frac{q^2}{m'} \right)^2 u_\sigma q \frac{1}{|u_\rho - u_\sigma|^3 q^3} \\
&\left\{ [\omega - u_\sigma q] [\omega - u_\rho q] \left[n_B \left[\frac{u_\rho[\omega - u_\sigma q]}{u_\rho - u_\sigma} \right] - n_B \left[\frac{u_\sigma[\omega - u_\rho q]}{u_\rho - u_\sigma} \right] \right] \right. \\
&- [\omega + u_\sigma q] [\omega + u_\rho q] \left. \left[n_B \left[\frac{u_\rho[\omega + u_\sigma q]}{u_\rho - u_\sigma} \right] - n_B \left[\frac{u_\sigma[\omega + u_\rho q]}{u_\rho - u_\sigma} \right] \right] \right\} \\
&- \frac{9}{\gamma_\sigma} \left[\gamma_\rho - \gamma_\sigma + \frac{1}{\gamma_\rho} - \frac{1}{\gamma_\sigma} \right] \frac{\omega}{u_\sigma q} \left(\frac{q}{m'} \right)^2 \frac{1}{|u_\rho + u_\sigma|^3} \\
&\left\{ [\omega + u_\sigma q] [\omega - u_\rho q] \left[n_B \left[-\frac{u_\sigma[\omega - u_\rho q]}{u_\rho + u_\sigma} \right] - n_B \left[\frac{u_\rho[\omega + u_\sigma q]}{u_\rho + u_\sigma} \right] \right] \right. \\
&- [\omega - u_\sigma q] [\omega + u_\rho q] \left. \left[n_B \left[-\frac{u_\sigma[\omega + u_\rho q]}{u_\rho + u_\sigma} \right] - n_B \left[\frac{u_\rho[\omega - u_\sigma q]}{u_\rho + u_\sigma} \right] \right] \right\}, \tag{D4}
\end{aligned}$$

$$\begin{aligned}
\Im\Sigma_C^R(\omega, q) &= \frac{9}{2u_\sigma\gamma_\sigma\gamma_\rho} \left[1 + \frac{\gamma_\rho}{\gamma_\sigma} \right]^2 \left[\frac{\omega}{u_\sigma q} \right]^2 \left(\frac{q^2}{m'} \right)^2 u_\sigma q \frac{1}{|u_\rho - u_\sigma|^3 q^3} \\
&\left\{ [\omega - u_\sigma q] [\omega - u_\rho q] \left[n_B \left[\frac{u_\rho[\omega - u_\sigma q]}{u_\rho - u_\sigma} \right] - n_B \left[\frac{u_\sigma[\omega - u_\rho q]}{u_\rho - u_\sigma} \right] \right] \right. \\
&+ [\omega + u_\sigma q] [\omega + u_\rho q] \left. \left[n_B \left[\frac{u_\rho[\omega + u_\sigma q]}{u_\rho - u_\sigma} \right] - n_B \left[\frac{u_\sigma[\omega + u_\rho q]}{u_\rho - u_\sigma} \right] \right] \right\} \\
&+ \frac{9}{2\gamma_\sigma\gamma_\rho} \left[1 - \frac{\gamma_\rho}{\gamma_\sigma} \right]^2 \left[\frac{\omega}{u_\sigma q} \right]^2 \left(\frac{q}{m'} \right)^2 \frac{1}{|u_\rho + u_\sigma|^3} \\
&\left\{ [\omega + u_\sigma q] [\omega - u_\rho q] \left[n_B \left[-\frac{u_\sigma[\omega - u_\rho q]}{u_\rho + u_\sigma} \right] - n_B \left[\frac{u_\rho[\omega + u_\sigma q]}{u_\rho + u_\sigma} \right] \right] \right. \\
&+ [\omega - u_\sigma q] [\omega + u_\rho q] \left. \left[n_B \left[-\frac{u_\sigma[\omega + u_\rho q]}{u_\rho + u_\sigma} \right] - n_B \left[\frac{u_\rho[\omega - u_\sigma q]}{u_\rho + u_\sigma} \right] \right] \right\}, \tag{D5}
\end{aligned}$$

where n_B is the Bose occupation function. Summing these contributions yields:

$$\begin{aligned}
\Im\Sigma_\sigma^R(\omega, q) &= \frac{9\gamma_\rho\gamma_\sigma}{2u_\sigma} \left[1 + \frac{1}{\gamma_\rho\gamma_\sigma} + \frac{1}{\gamma_\rho\gamma_\sigma} \left[1 + \frac{\gamma_\rho}{\gamma_\sigma} \right] \frac{\omega}{u_\sigma q} \right]^2 \left(\frac{q^2}{m'} \right)^2 u_\sigma q \\
&\frac{[\omega - u_\sigma q] [\omega - u_\rho q]}{|u_\rho - u_\sigma|^3 q^3} \left[n_B \left[\frac{u_\rho[\omega - u_\sigma q]}{u_\rho - u_\sigma} \right] - n_B \left[\frac{u_\sigma[\omega - u_\rho q]}{u_\rho - u_\sigma} \right] \right] \\
&+ \frac{9\gamma_\rho\gamma_\sigma}{2u_\sigma} \left[1 + \frac{1}{\gamma_\rho\gamma_\sigma} - \frac{1}{\gamma_\rho\gamma_\sigma} \left[1 + \frac{\gamma_\rho}{\gamma_\sigma} \right] \frac{\omega}{u_\sigma q} \right]^2 \left(\frac{q^2}{m'} \right)^2 u_\sigma q \\
&\frac{[\omega + u_\sigma q] [\omega + u_\rho q]}{|u_\rho - u_\sigma|^3 q^3} \left[n_B \left[\frac{u_\rho[\omega + u_\sigma q]}{u_\rho - u_\sigma} \right] - n_B \left[\frac{u_\sigma[\omega + u_\rho q]}{u_\rho - u_\sigma} \right] \right] \\
&+ \frac{9\gamma_\rho\gamma_\sigma}{2} \left[1 - \frac{1}{\gamma_\rho\gamma_\sigma} + \frac{1}{\gamma_\rho\gamma_\sigma} \left[1 - \frac{\gamma_\rho}{\gamma_\sigma} \right] \frac{\omega}{u_\sigma q} \right]^2 \left(\frac{q}{m'} \right)^2 \frac{1}{|u_\rho + u_\sigma|^3} \\
&[\omega + u_\sigma q] [\omega - u_\rho q] \left[n_B \left[-\frac{u_\sigma[\omega - u_\rho q]}{u_\rho + u_\sigma} \right] - n_B \left[\frac{u_\rho[\omega + u_\sigma q]}{u_\rho + u_\sigma} \right] \right] \\
&+ \frac{9\gamma_\rho\gamma_\sigma}{2} \left[1 - \frac{1}{\gamma_\rho\gamma_\sigma} - \frac{1}{\gamma_\rho\gamma_\sigma} \left[1 - \frac{\gamma_\rho}{\gamma_\sigma} \right] \frac{\omega}{u_\sigma q} \right]^2 \left(\frac{q}{m'} \right)^2 \frac{1}{|u_\rho + u_\sigma|^3} \\
&[\omega - u_\sigma q] [\omega + u_\rho q] \left[n_B \left[-\frac{u_\sigma[\omega + u_\rho q]}{u_\rho + u_\sigma} \right] - n_B \left[\frac{u_\rho[\omega - u_\sigma q]}{u_\rho + u_\sigma} \right] \right]. \tag{D6}
\end{aligned}$$

At $T = 0$ and in the limit where spin and charge parameters are equal ($\gamma_\sigma = \gamma_\rho$, $u_\sigma = u_\rho$) we recover the result of Eq. (27) with an additional factor of 2, *i.e.* the spin degeneracy. At $T = 0$ and in the absence of backscattering ($\gamma_\sigma = 1$, $u_\sigma = v$), Eq. (D6) reduces to Eq. (37).

-
- ¹ S.-I. Tomonaga, Prog. Theor. Phys. **5**, 544 (1950).
- ² J. M. Luttinger, J. Math. Phys. **4** 1154 (1963).
- ³ A. Luther and V. J. Peschel Phys. Rev. B **9**, 2911 (1974); S. Coleman Phys. Rev. D **11**, 2088 (1975).
- ⁴ F.D.M. Haldane, J. Phys. C **14**, 2585 (1981).
- ⁵ T. Giamarchi, "Quantum Physics in One Dimension", Oxford University Press, USA (2004).
- ⁶ A. O. Gogolin, A. A. Nersisyan and A. M. Tsvelik, "Bosonization and Strongly Correlated Systems", Cambridge University Press (2004).
- ⁷ D. Pines and P. Nozières, "The Theory of Quantum Liquids", Vol. 1, Perseus Books Publishing (1989).
- ⁸ F. H. L. Essler, H. Frahm, F. Göhmann, A. Klümper and V. E. Korepin, "The One-Dimensional Hubbard Model", Cambridge University Press (2005).
- ⁹ N. Andrei in "Low-Dimensional Quantum Field Theories for Condensed Matter Physicists", Series on Modern Condensed Matter Physics - Vol. 6, Edits. S. Lundqvist, G. Morandi and Yu Lu, World Scientific (1995).
- ¹⁰ F. H. L. Essler and V. E. Korepin, Phys. Rev. B **59**, 1734 (1999).
- ¹¹ N. Kitanine et al., hep-th/0505006.
- ¹² I. Affleck in "Fields, Strings and Critical Phenomena", Les Houches Session XLIX, Edits. E. Brézin and J. Zinn-Justin, Elsevier Science Publishers (1990).
- ¹³ S. Brazovskii, S. Matveenko and P. Nozières, J. Phys. I France **4**, 571 (1994); S. Brazovskii and S. Matveenko Sov. Phys. JETP **78**, 892 (1994).
- ¹⁴ K. V. Samokhin, J. Phys.: Cond. Matter **10**, L533 (1998).
- ¹⁵ M. Pustilnik et al., Phys. Rev. Lett. **91**, 126805 (2003).
- ¹⁶ A. G. Abanov and P. B. Wiegmann, Phys. Rev. Lett. **95**, 076402 (2005).
- ¹⁷ A. V. Rozhkov, Eur. Phys. J. B **47**, 193 (2005).
- ¹⁸ P. Pirooznia and P. Kopietz, cond-mat/0512494.
- ¹⁹ M. Pustilnik et al., Phys. Rev. Lett. **96**, 196405 (2006).
- ²⁰ R. G. Pereira, J. Sirker, J.-S. Caux, R. Hagemans, J. M. Maillet, S. R. White and I. Affleck, Phys. Rev. Lett. **96**, 257202 (2006).
- ²¹ S. Teber, Eur. Phys. J. B **52**, 233 (2006).
- ²² This agrees with our earlier result, derived in Ref. [21], that band-curvature only leads to sub-leading corrections to the electron self-energy: $\Im\Sigma \sim |\epsilon| + |\epsilon|^3/\epsilon_F^2$, where $\epsilon_F = mv^2$. The leading linear part is a signature that the electrons are not the stable quasi-particles of the system.
- ²³ The elementary excitations of the 1D liquid are the charge-less spin-1/2 spinon and the spinless charge $\pm e$ holon and anti-holon. They do not appear explicitly. Only pairs of these do. They correspond to the physical excitations of the system, see also [8,9]. In the spin sector they correspond to spin-singlet and -triplet excitations which are degenerate (they consist of two chargeless spin-1/2 spinons). In the charge sector they correspond to the charge-neutral holon-antiholon excitations otherwise known as particle-hole pairs. For technical reasons we keep the terminology particle-hole and reserve the one of holon-antiholon for the 1/2-filled case (the Bethe Ansatz description of the charge neutral excitations is different at 1/2-filling and below, see Ref. [8]).
- ²⁴ The elementary excitations of the system (holon, antiholon and spinon) interact with each-other as well as, below half-filling, with the incoherent background charge in the wire. This is apparent from our results for the charge and magnetic DSF, cf. Sec. III. This is also seen from the phase shifts associated with the scattering between these excitations and determined by the Bethe Ansatz solution to the Hubbard model, see Ref. [9]. *e.g.* the phase shift associated with the scattering between two spinons forming a singlet has one term describing pure spin scattering and another term, below half-filling, describing the scattering of a spinon off the incoherent background charge which is perturbed by the presence of the singlet.
- ²⁵ The model of spinful fermions is invariant under the large group: $U(1) \times SU(2)$, which has a non-Abelian component arising from the spin of the fermions. A rigorous procedure would require using the non-Abelian bosonization technique to treat the spin sector. This would yield the so-called $SU(2)$ level 1 Sugawara Hamiltonian and the corresponding Wess-Zumino-Witten (WZW) Lagrangian, see the textbook Ref. [6], properly generalized to include the effect of curvature. A formulation of the problem within the WZW non-linear σ -model is thus possible. In the present study, we restrict ourselves to a simpler Abelian bosonization and, whenever necessary, mention the constraints arising from the $SU(2)$ symmetry.
- ²⁶ In the literature on the Hubbard model both of these peaks are known, *e.g.* in Ref. [8] see Fig. 7.29 for the particle-hole peak and Fig. 7.31 for the singlet peak (the latter is degenerate with the spin-triplet).
- ²⁷ S. Teber (on progress).